Patrick Posch, BSc

Hydrothermal synthesized sodium titanates as anode materials in sodium-ion batteries

MASTER'S THESIS

to achieve the university degree of

Diplom-Ingenieur

Master's degree programme: Technical Chemistry

submitted to

Graz University of Technology

Supervisors

Univ.-Prof. Dr. rer. nat. Martin Wilkening

Institute for Chemistry and Technology of Materials

Dr. Ilie Hanzu

Institute for Chemistry and Technology of Materials

Graz, May 2016

Table of Contents

1. Abstract

The aim of this thesis is to investigate the performance of hydrothermal synthesized sodium titanates as anode materials in sodium ion batteries.

The hydrothermal synthesis method has already been used to form nano- or microstructured sodium titanates from $TiO_2 \cdot nH_2O$ gel, which is prepared using ammonia, hydrochloric acid and titanium tetrachloride, or Ti powder mixed with hydrogen peroxide and sodium hydroxide. The hydrothermal synthesis method featured in this thesis is based on TiO_2 nanopowder and sodium hydroxide which are simple and cheap educts.

The first part deals with the available electrodes and electrolytes for sodium ion batteries at the actual state of research. It also gives a quick insight in the competition with lithium ion batteries. Theoretical knowledge of the characterization methods will also be presented in the first part. The second part concentrates on the synthesis and characterization of the material. Morphologic studies are performed by scanning electron microscopy before using the material in half-cell test configuration.

Results show that further research is needed to enhance the performance of these materials for application in sodium ion batteries.

2. Sodium-Ion Batteries

2.1. Ecological View and comparison with Li-Ion Batteries

More efficient and cost effective energy storage systems will be needed to ensure a successful implementation of renewable energy systems into the already existing energy grid. Due to the fact that these renewable energies are nature dependent, they will neither deliver a constant nor a consumer based energy supply which makes new energy storage systems a necessity to ensure a constant power supply. The key features for these systems will be safety, lifetime, low/high temperature performance, availability and last but not least cost. During the last decades lithium batteries spread all over the world and sales went continuously up to high levels. Nowadays one quarter of the worldwide production of Li_2CO_3, the lithium precursor, is used for battery application and prices are rising even further. Meanwhile it is predicted that some lithium supplies and sources will expire in the near future. Even the recycled material from batteries that have reached their end-of-life will not cover the main part of the worldwide lithium demand, which will result in price fluctuations.[1]

On the other hand, battery research is more and more focusing on sodium due to its excellent availability and low costs. Sodium containing materials are capable of providing a battery system that might be competitive to lithium systems in the near future. Slater et al states: "The abundance of resources and the much lower cost of trona (about $135–165/ton), from which sodium carbonate is produced, compared to lithium carbonate (about $5000/ton in 2010), provide compelling rationales for the use of sodium in large scale battery applications, particularly in the near-term."[2] All of the early research projects on sodium based storage systems show similarities. These batteries are high temperature systems that have been investigated due to their high energy densities. The operation of those devices is very complex, since they usually require sodium in liquid state and utilize beta-alumina as electrolyte. In order to keep energy density, efficiency and lifetime at a maximum, these devices are operated at 300 to 350 °C. Hence, since

[1] Michael D. Slater, Donghan Kim, Eungje Lee, Christopher S. Johnson; Sodium-Ion Batteries; Adv. Funct. Mater. 2013, 23, 947-952
[2] Michael D. Slater, Donghan Kim, Eungje Lee, Christopher S. Johnson; Sodium-Ion Batteries; Adv. Funct. Mater. 2013, 23, 947

they have to be kept at high temperature to maintain continuous operation they are mainly suited for load leveling applications. [1]

The knowledge gathered during the past 20 years on lithium ion battery research is now applied to design sodium cells that are supposed to work similarly to lithium based systems. Even though sodium is less reducing (-2.71V vs. SHE for sodium and -3.04V for lithium) and shows a smaller theoretical capacity than lithium (1165mAh/g for sodium and 3829mAh/g for lithium), there are reports of sodium-tin cell systems that show higher volumetric capacities than the typical lithium setup.[3] These sodium-tin setups also provide further advantages, such as: lower cost associated with using aluminum current collectors instead of copper and improved safety through better thermal conductivity of the active metal electrodes. In order to find more suitable systems and to improve capacities, research groups are mainly focusing on finding adequate electrode materials. Nevertheless, the progress of these technologies will always be dependent on thermodynamical and mechanistic properties of charge storage, which determine energy density, reversibility, stability and reaction kinetics.[1]

2.2. Anode materials

2.2.1. Overview

To avoid systems containing pure sodium metal electrodes, materials with intercalated sodium ions are used in full cell approaches. The main reasons for these approaches are safety issues caused by the low melting point of sodium and its high reactivity. Unfortunately, at this stage of research, only a few suitable electrode materials are known and most of them have been tested in half cell arrangements with sodium metal counter electrodes. According to a simple classification we recognize carbon-based, metal oxide and intermetallic anode materials.[1]

2.2.2. Carbon-based anode materials

Carbon

Due to its low density and irregular layered structure, carbon black was one of the first materials to be investigated for application as electrode material in sodium-ion batteries. The high entropy of the structure has been verified by X-Ray Powder Diffraction (XPD)

[3] V. L. Chevrier, G. Ceder; Challenges for Na-ion Negative Electrodes; J. Electrochem. Soc. 2011 , 158

analysis, while Transmission Electron Microscopy (TEM) observation revealed agglomeration of primary particles in form of secondary structures in nanoscale size. Secondary structure sizes vary from 40 to 100 nm and appear in a round shape. These small particles are supposed to form a passivating layer at the electrode surface when being in contact with alkali metals. The reaction with sodium is known to happen at the surface of the electrode, since the porosity of the carbon black surface is almost negligible. Hence, insertion into the pores can be excluded from the overall activity of the material. Along with the Na_xSn-C material, irreversible capacities detected during the first cycles leaving evidence for the formation of a solid electrolyte interface. But unlike the lithium cell SEIs, the ones forming with carbon electrodes mostly consist of restructured carbon from the electrode surface. This characteristic has been proven by Alcántara et al. using FTIR spectroscopy and assigning the obtained peaks to the vibrations of organic groups. Other than that, half-cell experiments show that the solid electrolyte interphase (SEI) layer formed during the first cycles of a cell is in fact less protective and less passivating than the ones in lithium cells. In the case of a full cell consisting of a carbon black anode, a $Na_{0.7}CoO_2$ cathode (reversible capacity approximately 60 mA h g^{-1} vs. Na metal) and $NaClO_4$ (EC:DMC) electrolyte, a reversible capacity of 200 mA h g^{-1} can be achieved for carbon black.[4]

Compared to carbon black, hard-carbon is a material that provides an ordered structure also including a porous surface. BET measurements, using gas adsorption in order to determine surface area, show that carbon black reaches values of 22.1 up to 74.2 m^2 g^{-1} while hard-carbon only provides approximately 24 m^2 g^{-1}. When recording the first cycle capacities of both pure carbon materials, enormous differences can be observed since 308 and 540 mA h g^{-1} are measured for carbon black and hard-carbon respectively. Further cycling experiments deliver reversible capacities of averaged 96 mA h g^{-1} for carbon black and >300 mA h g^{-1} for hard-carbon. These reversibility differences are caused by the mechanism of sodium insertion into the material. While sodium is

[4] Alcantara, R.; Jimenez-Mateos, J. M.; Lavela, P.; Tirado, J. L., Carbon black: a promising electrode material for sodium ion batteries. Electrochem. Commun. 2001, 3, 639-642

occupying spaces between bent layers in the amorphous carbon black structure, it is way easier for the sodium ions to spread into the open pores of the hard-carbon structure.[5]

Na_xSn-C

Na_xSn-C is the evolution of hard-carbon electrodes which were the most popular anodes used in sodium-ion batteries. The small particle sizes of hard-carbon suggest determining the tapped density instead of the bulk density. Tapped density is determined by filling a graduated cylinder with the test material and tap the cylinder until no further volume change can be noticed. Due to the low tapped density of the material, and hence low overall volumetric energy density of the batteries equipped with hard-carbon, a composition of Sn-C was developed by Seung-Min Oh et al. The composite, consisting of tin nanoparticles embedded in an amorphous carbon matrix, is supposed to avoid aggregation and undergo no volume changes when inserting and extracting sodium ions. The application of hard-carbon instead of amorphous carbon would lead to aggregation and expansion and result in capacity fading of the material during operation. And even though no hard-carbon is used in the Na_xSn-C material, the tapped density is much higher than that of hard-carbon (3 g cm^{-3} vs. 0.9 g cm^{-3}). This material shows some irreversible capacity during the first cycles, which is due to solid electrolyte interphase layer formation at the electrode surface as well as rearrangement of the Sn-C structure when the alloy formation is about to begin. Under steady conditions operation at a capacity of 130 mA h g^{-1} is achieved, while the Coulombic efficiency remains 100% throughout the experiment.[6]

2.2.3. Metal oxide anode materials

$Na_2Ti_3O_7$, a material that has been reported in 1945 by B.F. Naylor[7] and has been studied for various applications in analytics or as toxic waste disposal agent, is now having its renaissance as active material in sodium cell electrodes. It features a multilayered titanium-oxygen structure that is capable of intercalating sodium ions. Lots of entirely different preparation methods are available, but the most common one is the typical

[5] Ponrouch, A.; Goni, A. R.; Palacin, M. R., High capacity hard carbon anodes for sodium ion batteries in additive free electrolyte. Electrochem. Commun. 2013, 27, 85-88

[6] Oh, S. M.; Myung, S. T.; Jang, M. W.; Scrosati, B.; Hassoun, J.; Sun, Y. K.; An advanced sodium-ion rechargeable battery based on a tin-carbon anode and a layered oxide framework cathode. PCCP 2013, 15, 3827-3833

[7] Naylor, B. F., High-Temperature Heat Contents of Na_2TiO_3, $Na_2Ti_2O_5$ and $Na_2Ti_3O_7$. J. Am. Chem. Soc. 1945, 67, 2120

mechanochemical synthesis using pure anatase TiO_2 and grinding it with some anhydrous Na_2CO_3. The mixture is then temperature treated at 800°C for 40 hours plus adding some regrinding breaks. A half-cell construction is achieved by mixing the obtained powder with 30% Super P carbon black and adding some 1M $NaClO_4$ in PC electrolyte as well as a pure sodium metal counter electrode. Stepwise potentiodynamic experiments confirm that a phase transition is occurring between two phases in a redox process manner. XRD analysis shows that the initial phase diminishes during the process and a new $Na_4Ti_3O_7$ phase is formed. During re-oxidation of the material a reformation of the initial $Na_2Ti_3O_7$ phase takes place, and the reduced form disappears completely as the oxidation process is finished. Electrochemical characterization reveals that $Na_2Ti_3O_7$ is capable of inserting sodium at voltages as low as 0.3V. The determined reversible capacity is 200 mAh g^{-1}, which is a high value for application in sodium ion cells.[8]

Another way to obtain the $Na_2Ti_3O_7$ material is hydrothermal synthesis. According to R.A. Zárate et al., product formation is achieved by mixing TiO_2 powder with highly concentrated NaOH solution in a Teflon beaker and heat it up to 130°C in an autoclave for a given period of time. Belt-like to wire-like nanostructures can be achieved by varying the sodium hydroxide concentration from 5M to 10M. XRD comparison shows that higher NaOH concentrations accelerate the formation of the titanate phase, since 5M NaOH experiments needed 6 days to develop titante phases compared to only 1 day of experiment duration with 10M NaOH as reaction agent. Scanning electron microscopy shows that using 5M NaOH as reagent leads to belt-like structures, dimensioning 8 to 40nm in width and 100nm to several µm in length, after one day of synthesis duration. The application of 10M NaOH as reaction agent for 18 hours yields wire-like structures with diameters from 8 to 10nm and lengths of several µm in a slightly dispersed order. Extending the reaction time will lead to higher diameters and shorter wires.[9]

[8] Senguttuvan, P.; Rousse, G.; Seznec, V.; Tarascon, J. M.; Palacin, M. R., Na2Ti3O7: Lowest Voltage Ever Reported Oxide Insertion Electrode for Sodium Ion Batteries. Chem. Mater. 2011, 23, 4109-4111

[9] Zárate, R.A.; Fuentes, S.; Wiff, J.P.; Fuenzalida, V.M.; Cabrera, A.L., Chemical composition and phase identification of sodium titanate nanostructures grown from titania by hydrothermal processing. Journal of Physics and Chemistry of Solids 2007, 68, 628–637

2.2.4. Intermetallic anode materials

Sn-Cu nanocomposites are attracting attention due to their improved stability compared to nanostructured tin electrodes. The synthesis is carried out at room temperature via a surfactant-assisted wet chemistry reaction. In the solution that is already containing the surfactant 1,2-diaminopropane, a reduction of Sn^{2+} and Cu^{2+} (ratio 9:1) is achieved by adding sodium borohydride. The composition of the obtained particles is determined $Sn_{0.9}Cu_{0.1}$. Nanostructured tin electrodes tend to agglomerate during the cycling process and are therefore losing capacity with progressive cycling. Intermetallic materials, such as $Sn_{0.9}Cu_{0.1}$, provide constant capacities and are therefore enhancing lifetime of the cells. From SEM observations the average particle diameter of the as-prepared material is found to be approximately 100nm and EDS identifies a homogeneous distribution of both elements and the ratio of Sn/Cu to be 0.896/0.104. Electrochemical cycling at 0.2C rate is performed in 2032 type coin cells with a slurry prepared anode consisting of 80% $Sn_{0.9}Cu_{0.1}$, 10% carbon black and 10% sodium carboxymethylcellulose binder, a sodium metal cathode and reference, as well as 1M $NaPF_6$ in FEC/DEC (1:1wt) electrolyte. Results show that the composite electrode experiences an extended initial sodium insertion process compared to tin (nano- and microstructured) active material electrodes. Even for cycle numbers up to 100, specific capacity of the composite remains constant. A direct comparison of reversible capacities gives 440 mAh g^{-1} for $Sn_{0.9}Cu_{0.1}$, 250 mAh g^{-1} for Sn nanoparticles and 66 mAh g^{-1} for Sn microparticles, shows that the tin copper composite exceeds the other two materials in capacity. Altering the charge/discharge rates from 0.2C to 0.5, 1 and 2C leads to high specific capacities of the $Sn_{0.9}Cu_{0.1}$ composite material (to 1694, 847 and 424 mAh g^{-1} respectively), while achieving lower specific capacities for the tin structures (265 ,182, 126 mAh g^{-1} for nano- and 222, 120, 50 mAh g^{-1} for microcrystalline tin respectively). Low first cycle Coulombic efficiencies indicate that $Sn_{0.9}Cu_{0.1}$ offers additional surface for SEI formation, which might be problematic in full-cells where cathode materials only provide a limited amount of sodium. The Coulombic efficiency of 99% reached after 100 cycles is still much lower than the 99.99% reversibility required in commercial cells. Post mortem analysis performed by EDS shows

bigger amounts of Na, F, O and C on the composite surface than on respective tin surfaces.[10]

Another composite investigated in the past years is SnSb/C. This material is based on the dispersion of tin and antimony nanoparticles into a nanostructured carbon phase. In the carbon matrix, tin and antimony form a single SnSb alloy phase that provides high capacities during cycling in sodium systems. Typical volume changes of the respective metals can be eliminated by preparing the afore-mentioned nanocomposite. Hence, the material provides reversible capacities of 544 mAh g^{-1} and maintains a Coulombic efficiency of more than 98 percent throughout the experiment. Due to the fact that both metals are participating equally in the alloying with sodium, a molar ratio of 1:1 for Sn and Sb is used for preparation.[11]

2.3. Cathode materials

Usually materials that can reversibly intercalate sodium ions at voltages higher than 2V positive to sodium metal are applied as cathode material in Na batteries. Materials with an operation window below 2 volts are used as anodes. Densely packed particles, high specific electrode capacities and increasing cathode voltage or decreasing anode working potential lead to an improved performance in sodium-ion batteries. Half-cell arrangements are limited by the stability of the sodium metal counter electrode, which tends to form dendrites and uneven surfaces when cycling exceeds 50 cycles. In order to improve cycling performance, a cathode material needs to show little to no volume change when inserting and exerting sodium ions. The available cathode materials for sodium cell application are limited by the atom coordination, since 6-coordinations like octahedral or prismatic structures are preferred for sodium insertion. Sodium coordination does not occur or is strongly limited in inorganic materials. The two main classes of cathodes are polyanionic networks that offer octahedral interstitials, and layered oxides which provide two dimensional stands for 6-coordinate intercalation of sodium. The polyanionics are divided into sulfides, fluorides, phosphates and sulfates.

[10] Lin, Y. M.; Abel, P. R.; Gupta, A.; Goodenough, J. B.; Heller, A.; Mullins, C. B., Sn-Cu Nanocomposite Anodes for Rechargeable Sodium-Ion Batteries. ACS Appl. Mater. Interfaces 2013, 5, 8273-8277

[11] Xiao, L; Cao, Y.; Xiao, J.; Wang, W.; Kovarik, L.; Nie, Z.; Liu, J., High capacity, reversible alloying reactions in SnSb/C nanocomposites for Na-ion battery applications. Chem. Commun. 2012, 48, 3321-3323

Nevertheless, most of the reported materials used for cathodes in these arrangements are oxides.

2.3.1. Polyanionic cathode materials

$Na_3M_2(PO_4)_2F_3$

These materials, in which the M spots are filled with either Titanium, Iron or Vanadium, are usually synthesized by solid-state synthesis or an ionothermal process according to N. Recham et al. The working principle of the solid-state method is the preparation of a mixture of V_2O_5, Ti_2O_3 or $FePO_4$ (anhydrous) with $(NH_4)_2HPO_4$ that is then annealed to 650-950°C for 15 hours in a crucible exposed to a 5% H_2 in Ar gas flow. Further calcination happens by adding a stoichiometric ratio of NaF and annealing at 600°C for 2 hours in Argon atmosphere. Alternatively, the ionothermal process is carried out at 270°C for 48 hours, followed by a centrifugation to separate product and ionic liquid which is then refurbished for the next synthesis. The educts used in the ionothermal process are stoichiometric amounts of M_3PO_4, MF_2, MCl_2 in a ratio of 1:0.5:0.5 as well as an ionic liquid consisting of 1,2-dimethyl-3-butylimidazolium bis(trifluoromethane-sulfonylimide).[12]

Solid-state synthesized charge/discharge experiments reveal that titanium and iron composites are low in capacity providing values of 57.7 and 43.66 mAh g^{-1}, respectively. Further, the titanium composite shows a small voltage gap of 0.3 V while the iron composite is lacking conductivity. The vanadium equivalent, on the other hand, provides a reversible capacity of 120 mAh g^{-1} with two voltage plateaus at 3.6 and 4.1 V. In a half-cell approach, cycling experiments show good cyclability between 2.3 and 4.6 V and a reversible capacity of 115.12 mAh g^{-1} that can be maintained throughout 40 cycles. In a full cell application, using a $NaTi_2(PO_4)_3$ anode, a reversible capacity of approximately 110 mAh g^{-1} is reached. Structural investigations, carried out via ex-situ X-ray diffraction, confirm volume changes during charging and discharging of the material. This can be observed by peak shifts occurring during the charging process, which undergo a backward shift to their original positions when discharging the material. The

[12] Recham, N.; Chotard, J. N.; Dupont, L.; Djellab, K.; Armand, M.; Tarascon, J. M., Ionothermal Synthesis of Sodium-Based Fluorophosphate Cathode Materials. J. Electrochem. Soc. 2009, 156, A995

electrochemical performance of the $Na_3V_2(PO_4)_2F_3$ compound can be described as excellent compared to the other sodiumfluorophosphate composites.[13]

$NaFeF_3$

This material, which is known as a Perovskite metal fluoride, has been investigated in the long run for sodium-ion battery approaches. Its preparation is dangerous due to the high reactivity caused by the enormous amounts of fluoride contained in the material. It is known to intercalate the sodium ions at the A sites in its ABO_3 structure, which can be seen in Figure 1. During the insertion process the present iron in the material is oxidized to Fe(II). Even though an extreme hysteresis can be observed on the charge / discharge curve, the voltage versus sodium is usually around 2 volts and during cycling at a low current rate of 0.2 mA cm^{-2} a capacity of 240 mAh g^{-1} can be reached. The material can be reversibly cycled between 1.5 and 4.5V in a sodium test cell.[1]

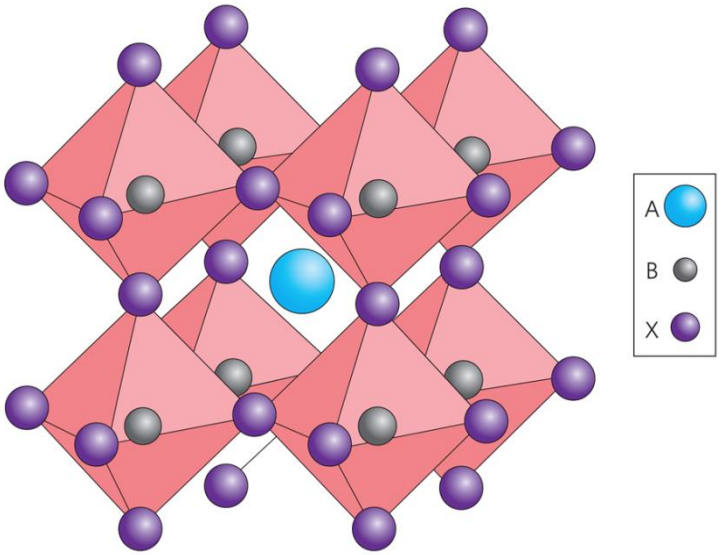

Figure 1 Structure of a generic Perovskite crystal [a]

[13] Chihara, K.; Kitajou, A.; Gocheva, I. D.; Okada, S.; Yamaki, J., Cathode properties of $Na_3M_2(PO_4)_2F_3$ (M=Ti, Fe, V) for sodium-ion batteries. J. Power Sources 2013, 227, 80-85

[a] Green, M. A.; Ho-Baillie, A.; Snaith, H. J., The emergence of perovskite solar cells. Nature Photonics 2014, 8, 506-514

2.3.2. Oxide cathode materials

$Na_xMo_2O_4$

The synthesis of this material has been published by McCarley et al. in 1985. Stating the reaction process to happen with a mixture of Na_2MoO_4 and $NaMo_4O_6$ powders, in a ratio of 6 to 5 respectively, at 900°C for several days in an evacuated electron beam welded copper tube. The reaction yields a black and well crystallized powder, which has been characterized by X-ray powder diffraction and differential scanning calorimetry. Results lead to a nominal composition of $Na_{1.33}Mo_2O_{4.22}$, which shows the same spectrum as $Na_2Mo_3O_6$ with two added peaks from a Na_2MoO_4 impurity phase.[14] Cycling in half-cells with a $Na_xMo_2O_4$, synthesized in either Pt or Cu tubes, show that Pt substrates yield higher sodium intercalation values. Further rinsing of the material with water only leads to loss of sodium, but is not affecting structural properties**.** Therefore the washed material reaches similar cycling values as the non-washed one. Both versions achieve a remarkably good reversibility of almost hundred percent, assembled as half-cells using dissolved 0.7M $NaClO_4$ in PC electrolyte. Nevertheless irreversible capacities, which can be explained by decomposition of electrolyte, are observed when operating the cell at values above 3.3V. The open circuit potential of these cells is 3V and delivers a theoretical capacity of 90 mAh g^{-1}.[15]

$Na(Ni_{0.5}Mn_{0.5})O_2$

In order to yield this material as reaction product, high-purity $NiSO_4 \cdot 6H_2O$ and $MnSO_4 \cdot 5H_2O$ need to be mixed in stoichiometric amounts and further dissolved in water to achieve a two molar concentration. The reaction is carried out in a continuously stirred tank reactor with nitrogen atmosphere, in which 2M NaOH solution and the needed amount of chelating agent NH_4OH are added. A careful monitoring of pH, temperature and agitation of the reaction mixture is necessary to obtain maximum yield. The intermediate is then dried and Na_2CO_3 is added, in a 1.02 molar ratio of Na/transition metals, before calcination is carried out at 820°C for 48 hours in air atmosphere. Composition analysis of the product is performed via XRD and results in the chemical composition $Na_{1.00}(Ni_{0.49}Mn_{0.51})O_2$. The main advantage of this material,

[14] McCarley, R.E.; Lii, K.H.; Edwards, P.A.; Brough, L.F., J. Solid State Chem. 1985, 57, 17

[15] Tarascon, J. M.; Hull, G. W., Sodium Intercalation into the Layer Oxides $Na_xMo_2O_4$. Solid State Ionics 1986, 22, 85-96

compared to the other available cathode materials for sodium-ion batteries, is the increased tapped density of almost 2.5 g cm^{-3}. As most of the other electrode materials, this composite shows volume changes when inserting sodium cations. This can be verified by observing the elongation of the a- and c-axis parameters of Na-O, M(Ni,Mn)-O as well as the distance of M-M structures. SEM reveals a spherical microstructure that is formed by sodiation during high temperature treatment. During cycling in a half-cell assembly, with $NaClO_4$ PC-FEC electrolyte, reversible capacities of 147 and 230 mAh g^{-1} can be achieved limiting the maximum voltage to 4 and 4.2V respectively. The higher voltage limit comes with better capacities, but unfortunately lowers the Coulombic efficiency to 93%. A Coulombic efficiency of 98.7% can be reached when cutting the potential at 4V. This behavior also indicates a deteriorating efficiency due to partial electrolyte decomposition in longer cycling experiments. A closer look on cycling speeds shows fading capacity with acceleration of the cycling process. Cycling at the speed of 1C yields a reversible capacity of 138 mAh g^{-1}, which reduces to 96 mAh g^{-1} at 10C.[4]

$Na(Ni_{0.33}Fe_{0.33}Mn_{0.33})O_2$

The synthesis is carried out by mixing $NiSO_4*6H_20$, $FeSO_4*7H_2O$, $MnSO_4*H_2O$ and $N_2C_2O_4$ with a co-precipitation agent in a vessel that is stirred at ambient air and 70°C for 3 hours. After filtering and drying the powder at 105°C, sodium carbonate is added in a 2:1 molar ratio and the resulting mixture is calcined at 850°C for 12 hours in air atmosphere. The exact stoichiometric molar ratios obtained with this synthesis method, investigated by ICP-OES, are 0.79:0.27:0.25:0.26 for Na:Ni:Fe:Mn respectively. XRD analysis indicates a single phase material with a α-$NaFeO_2$ structure, in which oxygen is stacked in ABC order following a hexagonally closest-packed structure. Sodium ions are occupying octahedral interstitials in one layer and the transition metals occupy interstitials in neighboring layers, resulting in a repeating pattern along the c-axis. In half-cells , versus sodium metal using 1M $NaClO_4$ in PC electrolyte, smooth and reversible sodium ion intercalation can be observed in a potential window from 2 to 4 volts. Further application in a full cell, with a hard-carbon anode and the afore-mentioned electrolyte, leads to an initial capacity loss of 28% caused by irreversible SEI formation at the carbon electrode. Nonetheless, these full cells perform fine due to their average voltage of -2.75V and yielding a reversible capacity of 100 mAh g^{-1} for 150 cycles at a charging rate of 0.5C. Setting a rate of 1C would even push the capacity to 150 mAh g^{-1}, but voltage recordings

indicate best intercalation performance at 94 mAh g^{-1} cathode capacity for 1C. Additionally, a coulombic efficiency of more than 99% over 150 cycles can be maintained when limiting the charging rate to 0.5C. XRD also states the cathode material layer to be intact after more than 120 cycles, all changes happening during discharge being completely reversible when recharging the material. All of these features describe this combination of electrodes as a very robust and extraordinary stable system that is also suitable for long-time applications.[16]

2.4. Electrolytes

The most popular formulations for liquid electrolytes applied in sodium-ion batteries are containing either $NaPF_6$ or $NaClO_4$ conductive salts dissolved in carbonate esters. Due to the fact that most anodic electrode materials show corrosion problems when being in contact with most of the commonly used carbonate ester solvents, the formation of a stability enhancing SEI is suppressed. The SEIs formed in lithium systems is necessary for stabilizing highly reducing electrode materials and might also be useful in sodium systems. A further problem with the widely used propylene carbonate as electrolyte basis in sodium systems is the formation of sodium propyl carbonate at the anode surface. This compound is then transported to the cathode where its oxidation takes place, leading to a decrease of Coulombic efficiency. In order to improve electrolyte efficiency, the development of electrode materials and electrolyte should be coupled. Latest electrolyte developments containing fluoroethylene carbonate show the formation of a passivating layer on both electrodes in a half-cell arrangement. Investigations reveal that side reactions are successfully prevented and an enhanced cycling performance can be observed for carbon anodes.[1] Ponrouch et al. focused on the performance of electrolytes in sodium systems by modifying the solvent composition. By using the same conductive salt concentration (1M $NaClO_4$) as well as to the same ethylene- (EC) to propylene carbonate (PC) ratio for all compositions, investigations show enormous differences in viscosity and ionic conductivity. Results show enhanced ionic conductivity in the following order DME>DMC>DEC added to an EC:PC (1:1) mixture in different quantities and using pure PC as reference. This trend can be observed at various temperatures. An adverse effect, noticeable by a decrease in conductivity, can be

[16] Kim, D.; Lee, E.; Slater, M.; Lu, W.; Rood, S.; Johnson, C.S., Layered $Na[N_{i0,33}Fe_{0,33}Mn_{0,33}]O_2$ cathodes for Na-ion battery application. Electrochemistry Communications 2012, 18, 66-69

obtained by adding more than 10%wt of DMC to the electrolyte mixture. Raman spectroscopy proves that adding less than 10%wt DMC to the electrolyte mixture does not contribute to cation solvation in the electrolyte. Raman spectroscopy results indicate that the enhanced conductivity of the mixed electrolyte is not an effect on the solvation shell in the electrolyte solution, but rather a change of viscosity.[17]

3. Galvanostatic cycling with potential limitation

Galvanostatic cycling with potential limitation, or its short form GCPL, is a form of chronopotentiometry in which current steps are applied to the electrodes. The potential that is recorded during the experiment changes its value in order to supply the current that is applied and causes a flux of electroactive species. A rapid potential change takes place after the transition time τ, as the current cannot be equalized by flowing redox species. The new potential value induces oxidation or reduction of species contained in the electrolyte. The transition time is determined by the Sand equation:

$$\tau^{1/2} = \frac{\pi^{1/2} n F D^{1/2} C^*}{2 i_0} \qquad \text{Eq. 1}$$

In which i_0 is the current density in [i/A], and the diffusion coefficient D is determined by a measurement of transition times at various current densities. In order to calculate an average value of the diffusion coefficient, this formula can be used:

$$D = \frac{4 i_0^2 \tau}{\pi (n F C^*)^2} \qquad \text{Eq. 2}$$

The two main advantages of chronopotentiometry experiments are the direct proportionality of the measured quantity τ and the diffusion coefficient D, as well as the independency of τ from heterogeneous electrode kinetics. The disadvantages are mainly caused by the planar electrode setup that causes convection at long experiment durations and charging current distorting the overall current. Selecting current densities that result in maximum transition times of 30 to 60 seconds will reduce the overall convection in the measurement setup. Current flows needed for the formation of a double-layer leading to a difference of Faradaic current and applied current, and

[17] Ponrouch, A.; Dedryvere, R.; Monti, D.; Demet, A. E.; Mba, J. M. A.; Croguennec, L.; Towards high energy density sodium ion batteries through electrolyte optimization. Energy. Environ. Sci. 2013, 6, 2361-2369

therefore result in inaccurate measurement of the transition time. But not only charging currents are complicating the measurement of τ in this setup, oxidation at the electrode surface and adsorbed electroactive species do also contribute to this problem. Determination of the diffusion coefficient is affected by short transition times, low concentrations and large capacitance electrodes that take part in the convergency of applied current and charging current. High interactions of these factors result in reduced accuracy. These are the main reasons why chronopotentiometry is not an established method for accurate diffusion coefficient measurements.[18] A refined method of chronopotentiometry called GCPL is also used for testing battery cells. This technique is taking advantage of potential limitation, which can prevent interactions with electroactive species in the electrolyte at high potentials. This enables the long-term investigation of battery setups in cycling experiments, as well as the determination of the reversibility of the intercalation processes going on during cycling, known as Coulombic efficiency.

4. Cyclic Voltammetry

The working principle of potential sweep methods, like cyclic voltammetry, is the forced change of electrode potential by an external source while recording the current. In these experiments a linear sweep can be applied to the test cell, resulting in a scan stop at a defined potential (E_2). In cyclic voltammetry measurements the applied potential sweep also includes a backward scan to E_1 or to even more negative potential values, as seen in Figure 2.

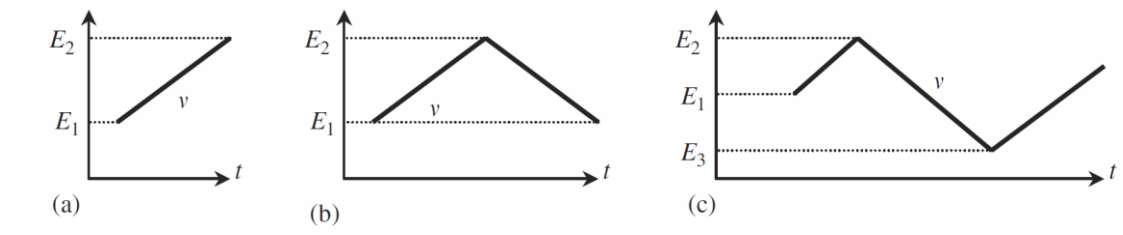

Figure 2 Waveforms in linear sweep (a) and cyclic voltammetry (b,c) experiments [b]

[18] Baur, J.E. in Handbook of Electrochemistry; Zoski, Cynthia G.,Ed;Elsevier:Amsterdam, 2007, 843-844
[b] Denuault, G.; Sosna, M.; Williams, K.-J. in Handbook of Electrochemistry; Zoski, Cynthia G.,Ed;Elsevier:Amsterdam, 2007, 438

Picking suitable waveform parameters is a necessity, since the potential extremes determine the electron transfer and oxidation state of involved species. Starting and reversal potentials also define whether the overall reaction is kinetic or mass transport controlled and if species are either formed or consumed during the process step. The potential sweep rate v is defined as the rate between two voltage steps and usually in a range of mV sec^{-1} to V sec^{-1}. The most interesting reaction parameters like kinetics and mechanism can be determined from the obtained current-voltage curves. Changing just a few parameters at the device, for investigation of an unknown material, results in lowered time-consumption for the operator. Cyclic voltammetry is always the first method that is used when investigating new electroactive materials. This method is widely used to determine complex reaction mechanisms including coupled homogeneous reactions or surface adsorption phenomena. Therefore a regular change in the applied waveform is used to obtain differently shaped voltammograms. When analyzing the voltammograms, the focus is set on the number of peaks, their shapes, their sizes and most of all their positions. Figure 3 shows a typical cyclic voltammogram in which different points of the curve are numbered to label concentration changes that are taking place at the electrode surface. While points 1 to 7 demonstrate a reduction of the oxidized species at the electrode surface, points 8 to 10 show the associated regeneration of the oxidized species from the reduced one. The sign change of the current is a consequence of the change in concentration of the oxidized species at the surface. The expression describing this process is Fick's first law of diffusion, which states that the current flow is proportional to the concentration gradient at the electrode. A very important equation, describing the planar-diffusion controlled case, is the Randles-Sevčik equation (Eq. 3). It demonstrates proportionality between the peak current and the square root of the sweep rate. Applying this equation by plotting i_p vs. $v^{1/2}$ leads to a

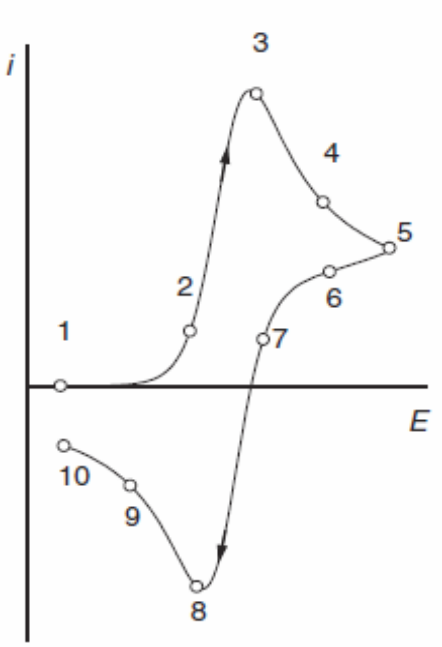

Figure 3 Typical cyclic voltammogram with marked spots along the curve [c]

linear dependency that passes the origin and the diffusion coefficient can be estimated from its gradient.

$$i_P = 0.4463 \frac{n^{3/2} F^{3/2}}{R^{1/2} T^{1/2}} A D_0^{1/2} C_0^* v^{1/2} \qquad \text{Eq. 3}$$

The difference in potential of the anodic and cathodic peak at 298K is always 59mV divided by the number of electrons participating in the redox reaction. When the rate of mass transport exceeds the rate of electron transfer, a significant change in voltammogram shapes can be observed. If both values, mass transfer coefficient and electron transfer rate, are equal or comparable to each other a typical diffusion-controlled voltammogram can be obtained. At high scan rates, leading to an increase in mass transfer coefficient, the voltammogram curve is stretched in x-direction. In order to achieve comparable electron transfer values, the overpotential needs to be higher and broadened, more separated peaks occur. The more the mass transport coefficient increases, the less reverse peak can be detected. In irreversible systems the values of mass transport are way higher than those of the electron transfer, leading to a complete disappearance of the reverse peak. The effect of decreasing electron transfer rate is depicted in Figure 4.[19]

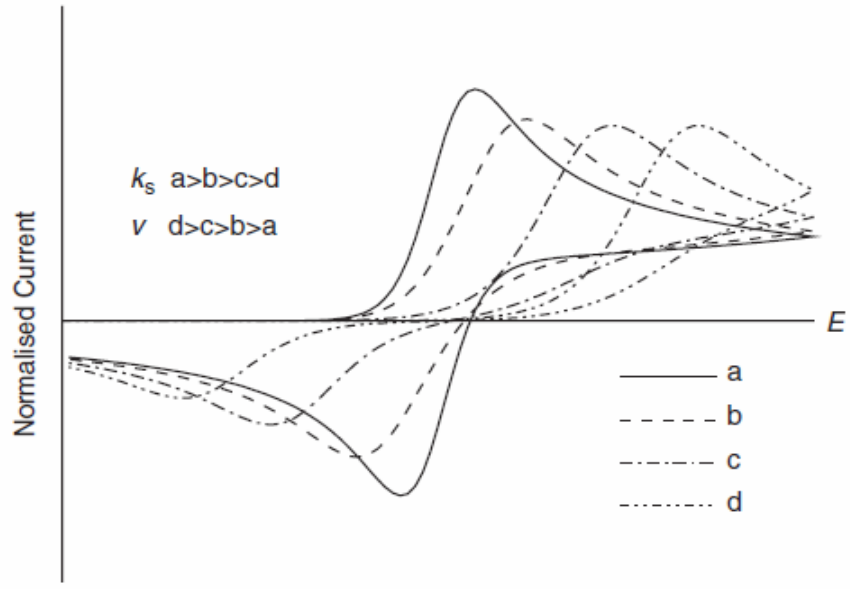

Figure 4 Voltammogram comparison of different scan rates and electron transfer rates [d]

[19] Denuault, G.; Sosna, M.; Williams, K.-J. in Handbook of Electrochemistry; Zoski, Cynthia G.,Ed;Elsevier:Amsterdam, 2007, 438-441

[c] Denuault, G.; Sosna, M.; Williams, K.-J. in Handbook of Electrochemistry; Zoski, Cynthia G.,Ed;Elsevier:Amsterdam, 2007, 439

[d] Denuault, G.; Sosna, M.; Williams, K.-J. in Handbook of Electrochemistry; Zoski, Cynthia G.,Ed;Elsevier:Amsterdam, 2007, 441

5. X-ray diffractometry

X-ray diffraction is a fast analytical method that is primarily used to identify the different phases of a crystalline material. Crystal structures can be gathered by measuring unit cell dimensions. In order to perform measurements the X-rays are generated by a cathode ray tube (CRT), filtered and collimated before they hit the target. The fundamental principle of these measurements is interference between the monochromatic X-rays and the crystalline sample. Interaction between rays and crystalline surface will be constructive when the conditions of Bragg's law (Eq. 4) are met.

$$n\lambda = 2d \cdot \sin(\theta) \qquad \text{Eq. 4}$$

Bragg's law links wavelength (λ) of the radiation to the lattice spacing (d) of the sample. It is possible to detect all diffraction directions of the samples crystal lattice by scanning diffraction angles through the range of 2θ. Each mineral has a unique set of peaks that are obtained via X-ray diffraction and correlate to their individual crystal lattice spacing. The obtained spectra are then compared to the ones found in international databases for crystal structures, such as: Inorganic Crystal Structure Database (ICSD) or Cambridge Crystallographic Data Center (CCDC). A typical powder XRD spectrum of Germanium can be seen in Figure 5.[20]

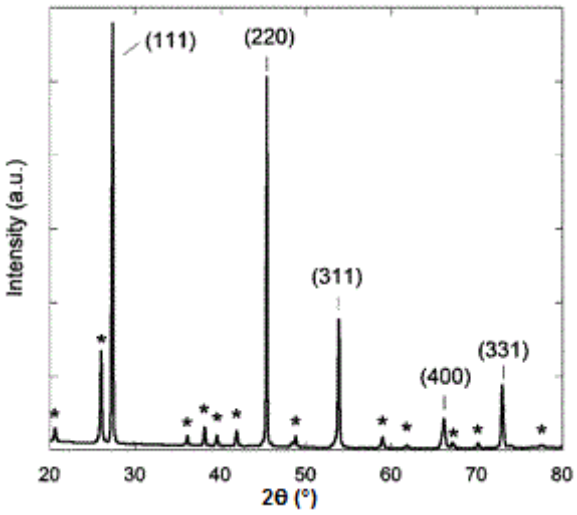

Figure 5 XRD powder pattern of Germanium [e]

[20] Brown, T.L.; LeMay, H.E.; Bursten, B.E. in Chemistry: The Central Science; Pearson Education, Inc.:München, 2006, 545

[e] Chiu, H. W.; Chervin, C. N.; Kauzlarich, S. M.; Phase changes in Ge nanoparticles. *Chem. Mater.*, 2005, 17, 4858

6. Experimental Part

6.1. Experimental Setup

This work focuses on sodium titanium oxides (Na_xTiO_2). The sodium titanium oxides tested in sodium ion batteries are synthesized by a hydrothermal method from two simple educts named TiO_2 and NaOH. The TiO_2 is delivered by SIGMA-ALDRICH in nano-powder form with an average particle size lower than 5nm, while the NaOH is provided in pellet form by SIGMA-ALDRICH. After dissolving the NaOH pellets in an appropriate amount of Millipore water to obtain a 10 M solution, the two educts are mixed in a PTFE autoclave beaker by stirring for 20 minutes. The exact composition of the mixture before hydrothermal reaction can be seen in Table 1. The obtained white suspension is then placed in an autoclave and kept at 165°C for 72 hours.

Table 1 Hydrothermal synthesis educts

Reagent	TiO_2	NaOH
Mass	20g	6g
Ratio	3.33:1	

After the cooldown phase, a greasy white solid cylinder can be removed from the autoclave beaker. This material is then split and stirred at ambient temperature with 200 mL of 0.1M $(NH_4)_2CO_3$ for two hours. The flakes, resulting from the detaching of particles from the solid block during rinsing process, are then filtrated and the rinsing step is repeated several times. After each rinsing step the pH value is checked with a pH indicator paper. The different fractions of the sample are going through varying numbers of rinsing steps, from two to seven. A 48 hours drying process at 60°C and ambient pressure is carried out after the last filtration step. Afterwards the samples are divided into 6 parts and annealed at different temperatures in 100°C steps from 350 to 850°C. The annealing process is carried out in a muffle furnace using the following uniform heating pattern for all experiments: ramping 120°C/hour to the desired annealing temperature, keeping the temperature for 4 hours and cool down by turning off the heating element. The annealed samples are used to prepare slurries consisting of 70% Na_xTiO_2, 20% Super C65 and 10% Sodium Carboxymethylcellulose WALOCEL CRT 2000 PA 07 provided by Wolff Cellulosics GmbH & Co.KG (1.25%wt dissolved in Millipore water). The thoroughly stirred slurries are then cast on 50µm thick copper foils with a casting gap of 100 µm. After 12 hours of drying in a Memmert drying oven at 60°C and ambient

pressure, electrodes with a diameter of 10 millimeters are punched out of the coated copper foil. These electrodes undergo further drying at 120°C and 10^{-3} mbar pressure for at least 12 hours before weighing them, with a METTLER-TOLEDO XA105 DualRange analysis balance, to determine the active mass of each electrode. Further drying is performed by high vacuum equipment that maintains 120°C and $2*10^{-6}$ mbar for at least 36 hours. Finally the dried electrodes are assembled in 3-electrode Swagelok cells using metallic sodium as counter- and reference-electrode and 1M $NaClO_4$ dissolved in propylene carbonate as electrolyte. The Swagelok cell assembly is depicted in Figure 6. The assembled cells are then used for galvanostatic cycling and cyclovoltammetry experiments carried out with a BIOLOGIC MPG-2 device. Surface investigation is carried out by Scanning Electron Microscopy (SEM) combined with energy-dispersive X-ray spectroscopy (EDX) for determination of the composition. In addition, X-ray diffraction (XRD) measurements of the treated powders are performed aiming to determine the composition of the Na_xTiO_2 active material.

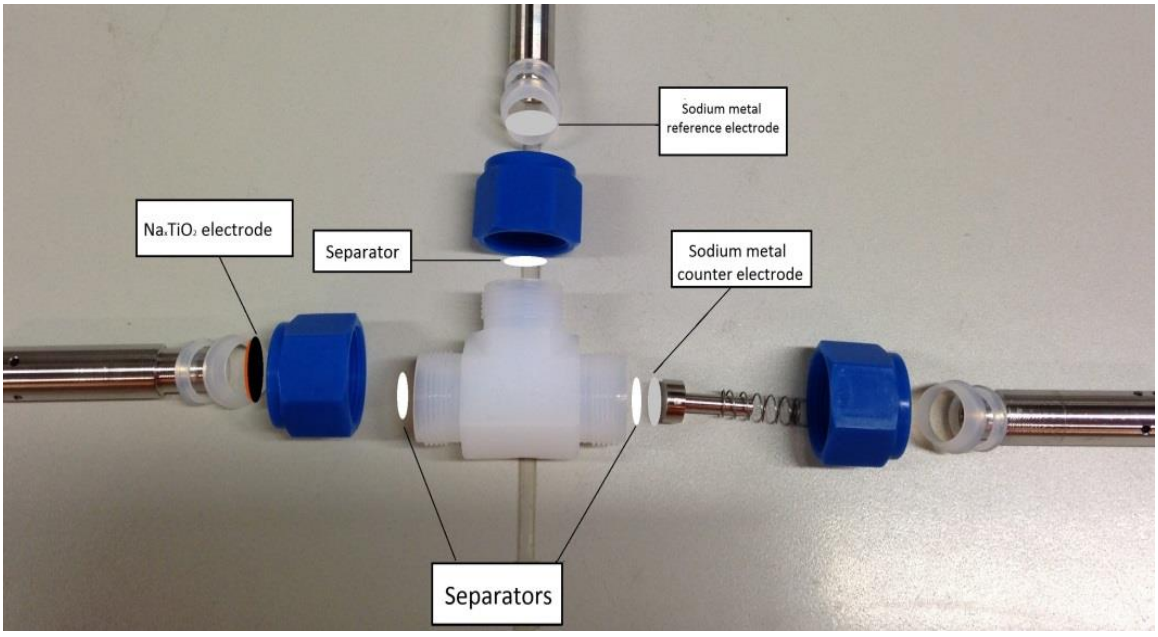

Figure 6 Swagelok 3-electrode cell assembly

6.2. Experimental Results

6.2.1. Annealing Process

The samples are dried for at least 48 hours directly after the last rinsing step, which would lead to the assumption that the weight caused by wet samples is negligibly small. Nevertheless, a comparison of the sample weights before and after the annealing process reveals a mass loss for every sample. Some samples lose up to 41% of mass during the annealing process. Homogeneous sample mass loss can be observed for 2,6 and 7 times rinsed samples, while those that have been rinsed 3,4 and 5 times show a deviation in mass loss of up to 7%.

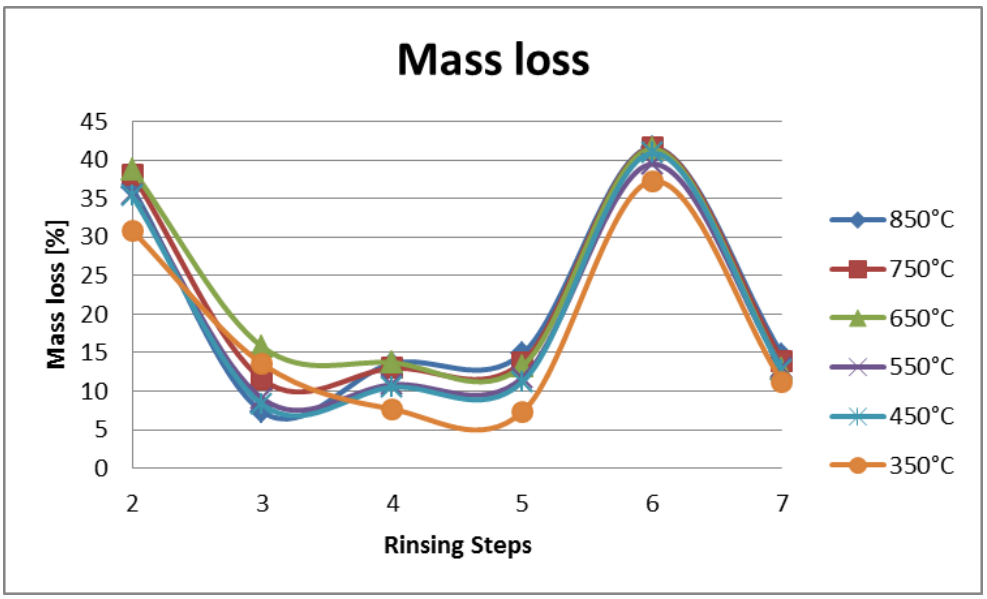

Figure 7 Mass loss during annealing process as a function of rinsing step number (lines are used to guide the eye)

The mass loss related to the annealing of the sample is supposed to happen due to conformation and composition changes, since (except for 2 and 3 times rinsed samples) the change in mass rises with rising temperature, as shown in Figure 7. An additional fact that can be observed immediately after the annealing process is the color change of some samples. Samples that are annealed at temperatures from 550 to 850°C keep their original white color. On the other hand, samples that are annealed at 350 and 450°C and rinsed with 0.1M $(NH_4)_2CO_3$ more than 4 times shift to cream color. This effect is shown in Figure 8 and Figure 9.

Figure 8 Samples annealed at 850°C

Figure 9 Samples annealed at 450°C

Further influences of the annealing temperature on the microstructure of the material can be seen in the SEM investigation and electrochemical analysis data.

6.2.2. Scanning electron microscopy

Scanning electron microscopy analysis is carried out to investigate the surface of the hydrothermally synthesized Na_xTiO_2 powder. First investigation focusses on the differences in surface properties according to different rinsing solvents. Figure 10 depicts a comparison of 0.1M $(NH_4)_2CO_3$, water and ethanol rinsed samples that have been annealed at 350°C with a magnification of 5,000. Figure 11 zooms in even further and the differences in microstructure can be seen at a magnification of 20,000.

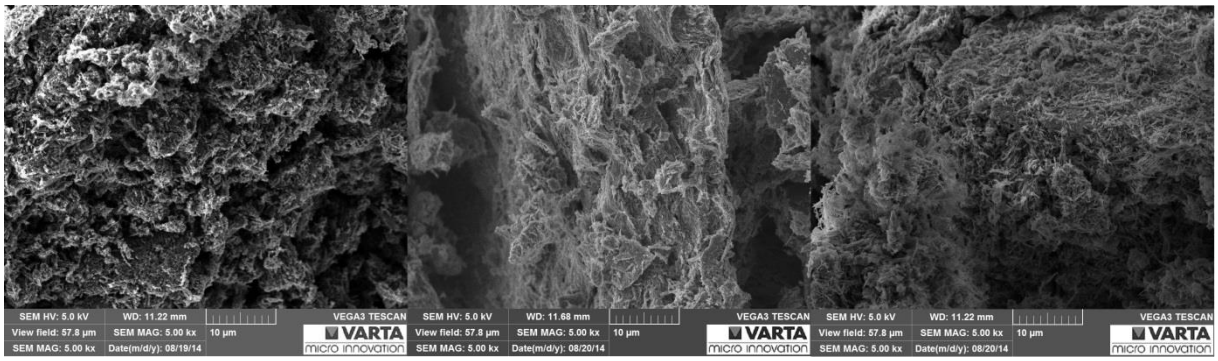

Figure 10 Comparison of 0.1M $(NH_4)_2CO_3$, water and ethanol rinsed samples (left to right). Magnification: 5,000

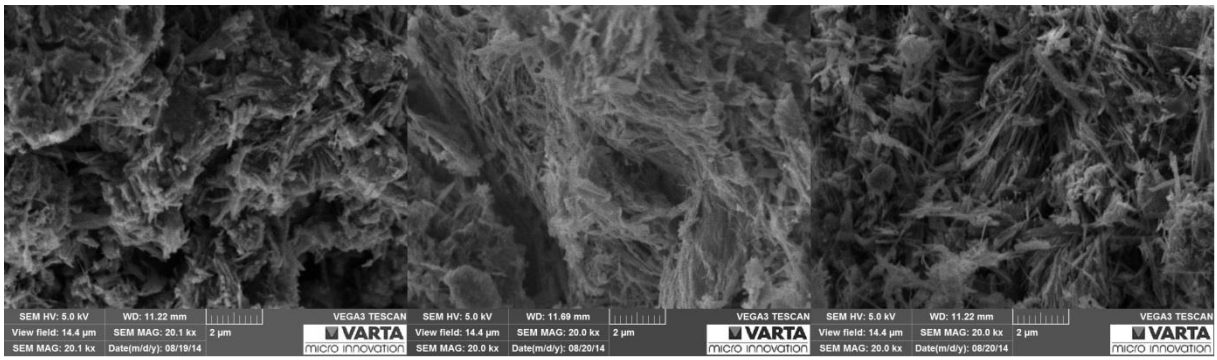

Figure 11 Comparison of 0.1M $(NH_4)_2CO_3$, water and ethanol rinsed samples (left to right). Magnification: 20,000

An increase in porosity from water to ethanol/0.1M $(NH_4)_2CO_3$ rinsed samples can be noticed when comparing the images acquired at a magnification of 5,000. This is even more obvious when comparing the micrographs acquired at higher magnification. The rod-structure obtained from the synthesis process expands when rinsing with 0.1M $(NH_4)_2CO_3$ or ethanol, leading to the formation of wider channels throughout the surface. Further investigations show that the number of rinsing steps, as well as the annealing temperature, influence the size of the formed microrods. Samples undergoing only 2 rinsing steps with 0.1M $(NH_4)_2CO_3$ and an annealing process at 350°C show a larger scale conglomerate of rods and particles, than the as-prepared sample annealed at 850°C (seen in Figure 12).

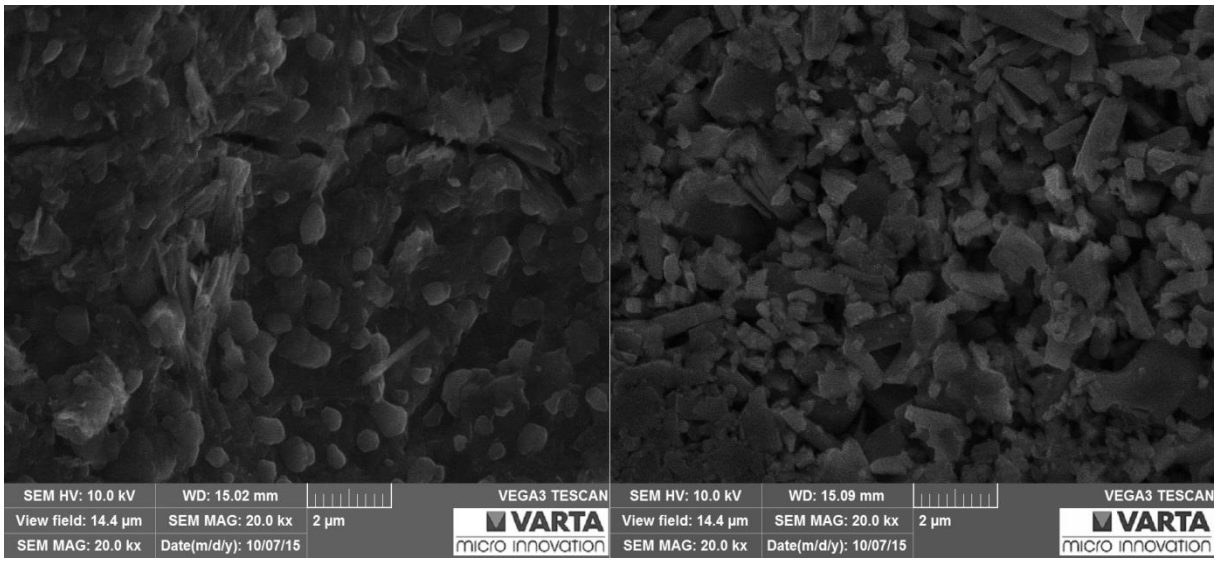

Figure 12 SEM Comparison of 2 annealing temperatures: 350°C(left) and 850°C(right). Magnification: 20,000

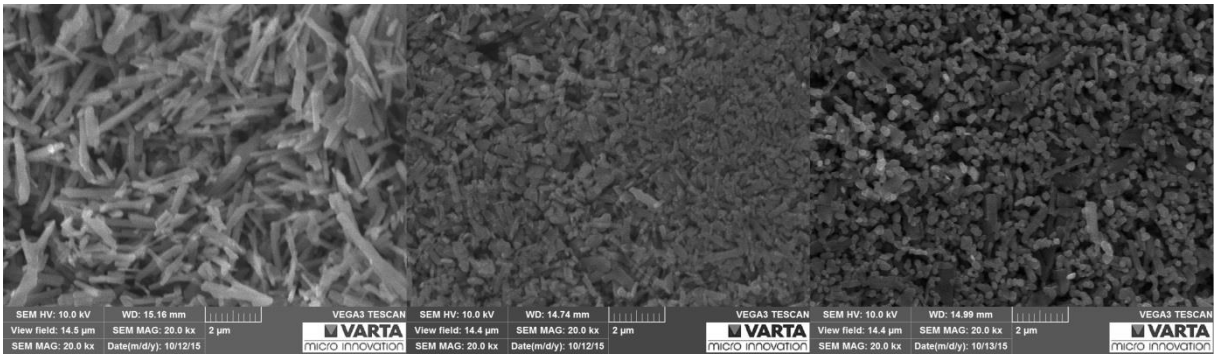

Figure 13 SEM Comparison of different rinsing repetitions at annealing temperature 850°C

In order to determine the influence of the rinsing repetitions, samples with different amounts of rinsing steps are annealed at the same temperature and pictures of the powders are taken. In case of Figure 13 the samples are rinsed 3,4 and 6 times with 0.1M $(NH_4)_2CO_3$ and all of them are annealed at 850°C. This comparison proves that the microrod length decreases with increasing rinsing repetitions, but also increases the organization of the rods.

6.2.3. Energy-dispersive X-Ray spectroscopy

EDX spectroscopy is performed in order to determine the surface composition of the target during SEM investigations. It provides quick and exact data at a self-picked spot on the surface and does not contain any information of the bulk or overall composition of the sample, but gives a brief impression what the overall composition might be. Table 2 shows the differences between the investigated samples. It can be seen that the sodium content built up by the synthesis method decreases with increasing rinsing repetitions. Carbon is detected because of the conductive carbon adhesive tape.

Table 2 EDX analysis of the different samples given in Weight%/Atomic%

	Rinsing repetitions						
Element	**2**	**3**	**4**	**5**	**6**	**7**	
C	2.48/4.94	1.10/2.17	1.35/2.71	2.23/4.67	3.27/6.68	1.06/2.44	**350°C**
O	39.44/59.11	43.33/64.44	44.53/66.83	39.32/61.94	41.10/63.07	33.31/57.63	
Na	12.68/13.22	10.74/11.11	6.14/6.41	4.62/5.06	3.13/3.34	3.2/3.85	
Ti	45.40/22.73	44.84/22.28	47.98/24.05	53.84/28.33	52.50/26.91	62.44/36.08	
C	1.39/2.6	0.24/0.52	0.31/0.66	0.90/1.91	0.16/0.35	0.07/0.14	**850°C**
O	45.83/64.11	36.33/59.31	40.43/64.27	40.65/64.34	42.86/68.28	42.08/66.80	
Na	17.06/16.61	9.47/10.75	6.26/6.92	4.99/5.50	1.84/2.04	4.16/4.60	
Ti	35.71/16.68	53.97/29.42	53.00/28.14	53.46/28.26	55.13/29.33	53.69/28.46	

A comparison of the effect caused by the different rinsing media is also performed by EDX measurements. Table 3 shows the results and it can be seen that the highest sodium content kept in the material is achieved by rinsing with ethanol.

Table 3 EDX comparison between different rinsing media

	0.1M NH_4CO_3	**Water**	**Ethanol**
C	6.12	3.12	10.81
O	67.38	60.86	60.94
Na	8.36	9.36	14.69
Ti	18.14	26.65	13.56

A typical spectrum obtained by EDX spectroscopy is shown in Figure 14. It connects the energy in kilo electronvolt on the abscissa with the count number on the ordinate. Due to known energies the peaks can be linked to chemical elements, which is done automatically by the program by assigning the peaks to their corresponding energy from a database. It can be seen from the spectrum that the majority of elements is marked as either titanium or oxygen, which is due to the main component TiO_2, but carbon and sodium are detected as well. Sodium ought to be found in this material since it is

intercalated during the synthesis process and is an important component of the material. Carbon, on the other hand, might not be part of the sample itself but rather an artifact from the conducting duct tape that, to a large extent, consists of carbon.

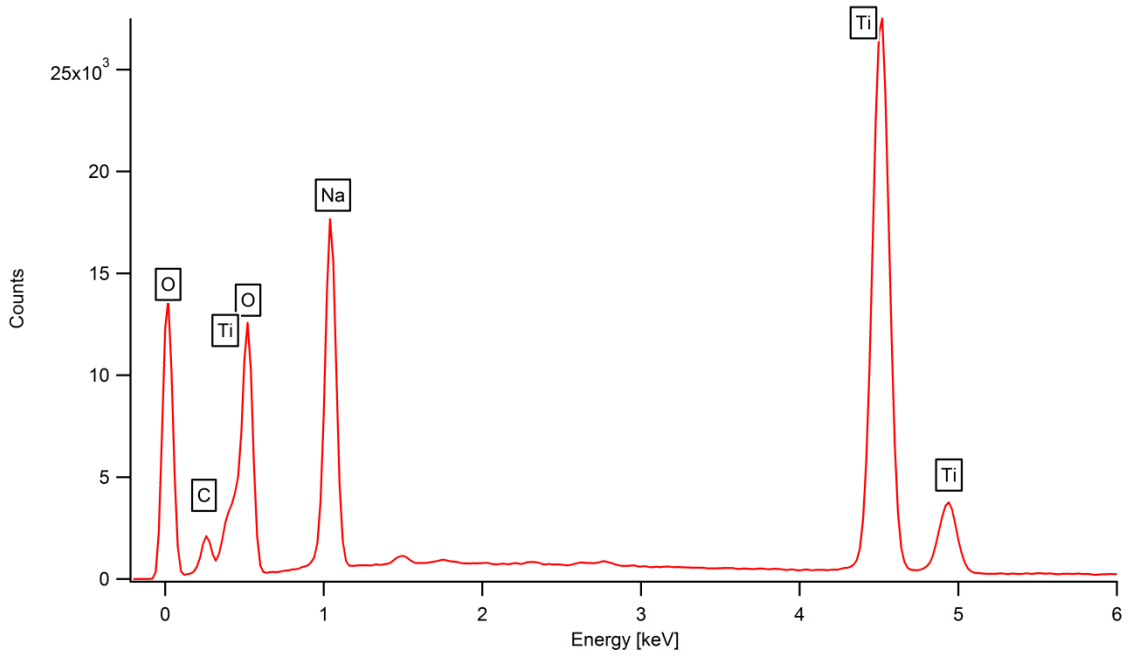

Figure 14 EDX spectrum of ethanol rinsed and annealed (350°C) Na_xTiO_2

6.2.4. Cyclic Voltammetry

Cycling voltammetry measurements are performed to follow the redox processes taking place at the test electrodes. In order to enhance visibility of the processes, the sweep potential is alternated throughout the process. Table 4 shows the changes in scan rate during the measurements.

Table 4 Cyclic voltammetry experiment scan rate

Cycles	1st	3rd	5th	7th	9th	11th	13th	15th
Scan rate [mV/s]	0.02	0.1	0.2	0.5	1	2	5	10

The higher the scan rate, the higher the recorded current response. This usually leads to larger peaks as well as distortion effects, which may be caused by instability of the electrode material at very high currents. Figure 15 depicts a comparison of six samples that have been annealed at 850°C but differ in rinsing repetitions. In order to get rid of irreversibilites and show comparable reversible results, the graph pictured in Figure 15 only includes data gathered during the second cycle. The disappearance of an electroactive phase can be observed when raising the number of rinsing steps.

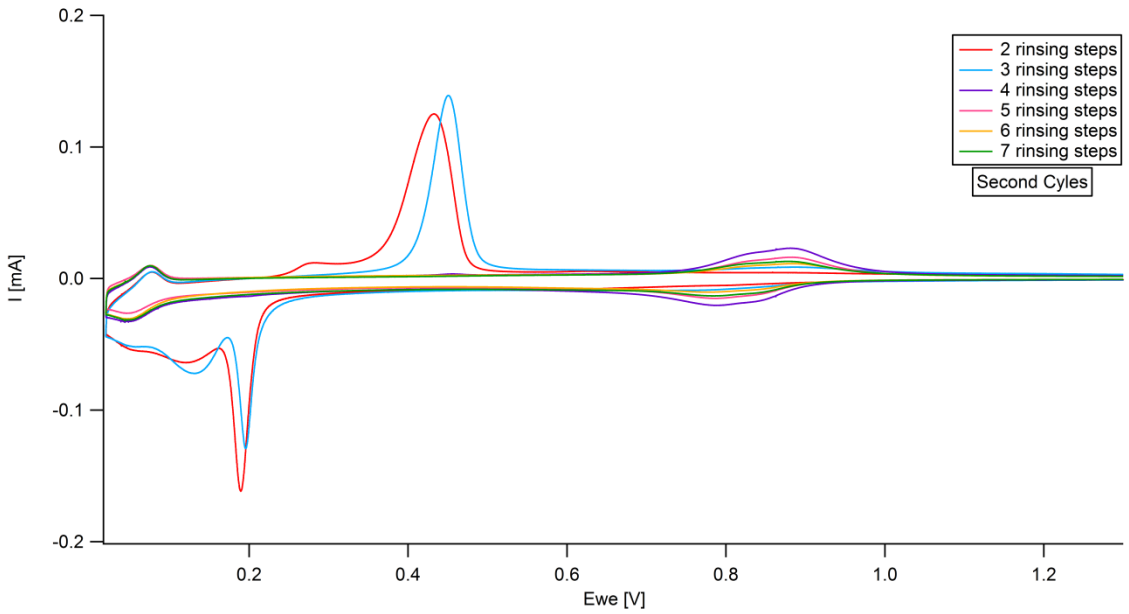

Figure 15 CV (second cycle) comparison of samples annealed at 850°C

Figure 16 shows exactly the same samples during their first cycles. Especially the samples rinsed less often show significant irreversible capacities during the first reduction process. This can clearly be seen in the reduction area below 0.2 volts. This behavior is known for irreversible changes in the electrode material during the first reduction of the

material. The unsurprising fact that larger irreversible capacities are obtained for samples with less than 4 rinsing repetitions, is explained by the higher sodium content of those samples (see 6.2.3). On the other hand Figure 17 shows that the peaks of an additional phase, which is obtained when lowering the number of rinsing repetitions to 2 or 3, seem to be reversible throughout the sweep rate variations. It can also be seen that during the last two cycles the peak shoulder merges to a broad single peak. One can also notice that no reactions are occurring above 0.7V, which indicates that the 2 times rinsed sample which has been annealed at 850°C has a completely different composition than the ones that are rinsed more often. Samples that have been rinsed more than 3 times do not show any outstanding reversible reactions in the voltage range from 0.15 to 0.6V. Figure 18 compares the second cycles of samples undergoing two rinsing repetitions to show differences caused by annealing temperature.

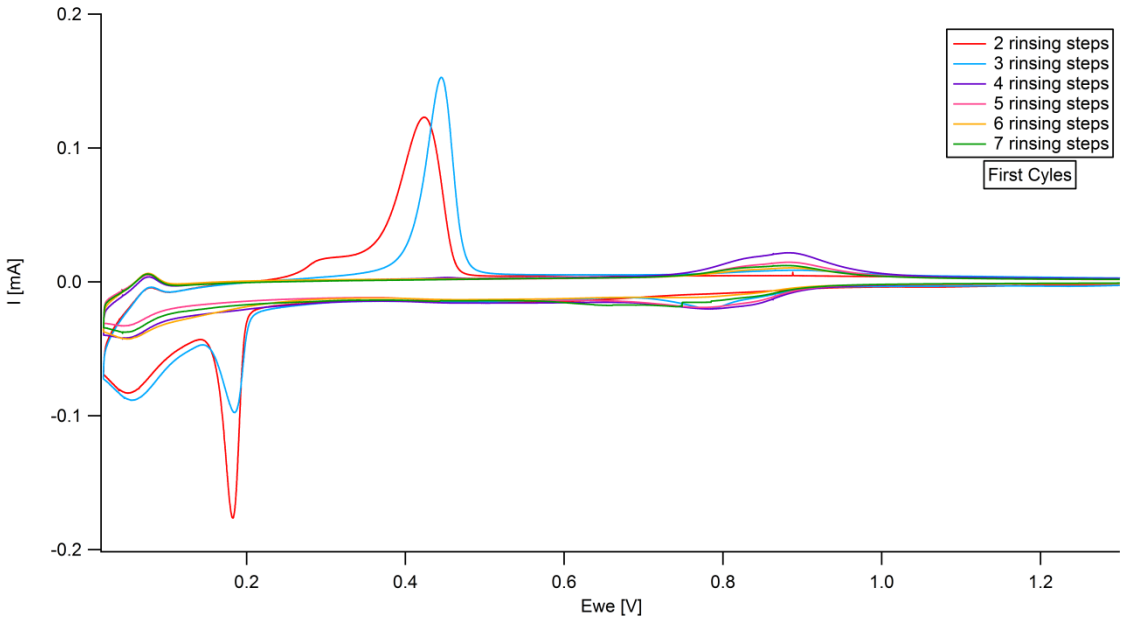

Figure 16 CV (first cycle) comparison of samples annealed at 850°C

It can be seen that the material phase that shows electrochemical activity at 0.43V (reduction) and 0.19V (oxidation) only occurs in samples that are annealed at a temperature of at least 650°C. Peak maxima of the three samples that show this behavior are matching, even though it can be seen that smaller peaks next to the discussed ones, at 0.28V reductive and 0.12V oxidative, do not match. The sample annealed at 650°C seems to be a mixture between the sample obtained at 550°C and 750°C annealing temperature, since there are a lot of matching peaks on both sides.

A formation of a different phase seems to be dependent on annealing temperature as well as rinsing procedure. Further investigations on this effect are performed by XRD measurements.

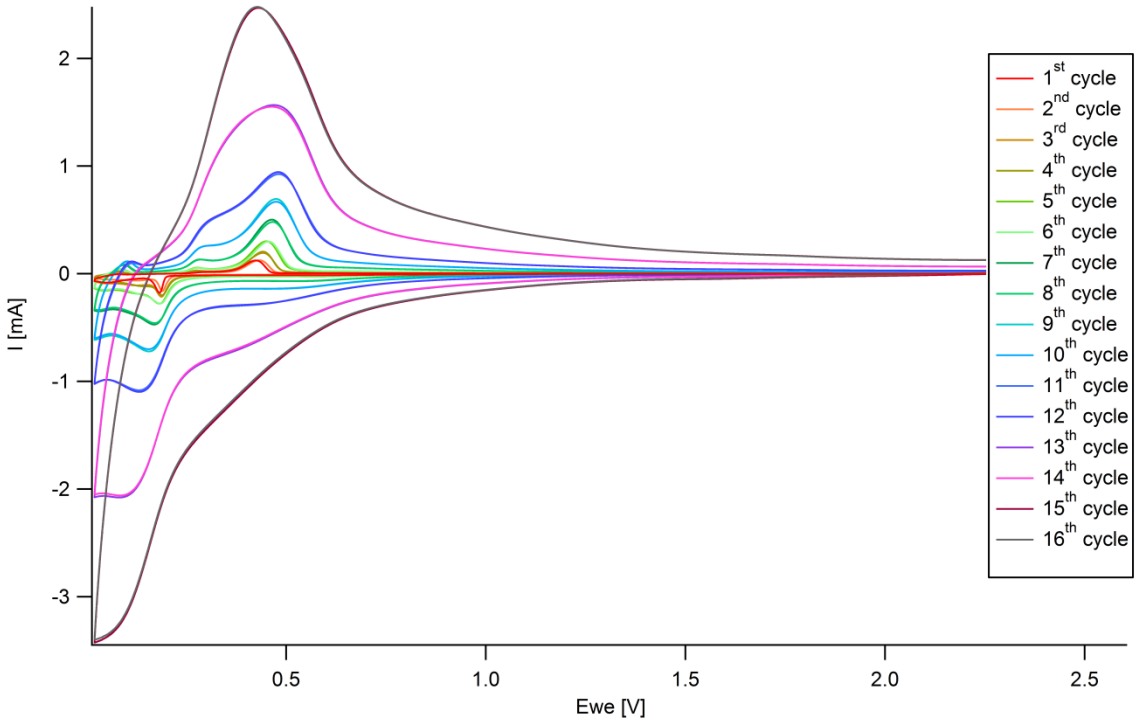

Figure 17 Cyclic voltammetry measurement of a 2 times rinsed sample which is annealed at 850°C

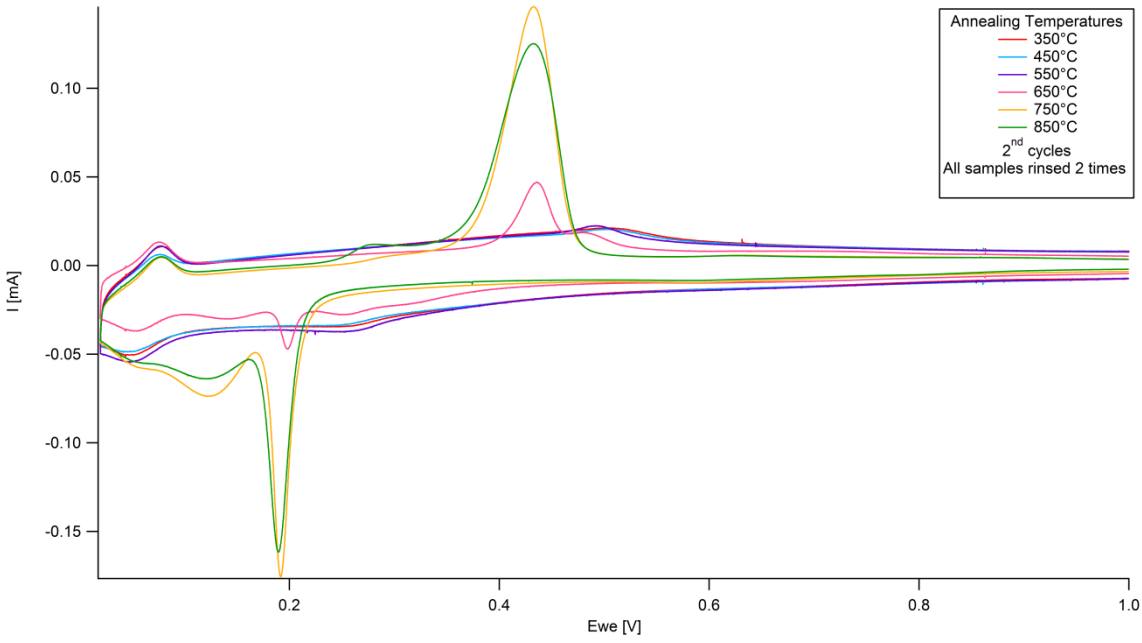

Figure 18 Cyclic voltammograms depicting 2nd cycle of samples rinsed 2 times and annealed temperatures from 350 to 850°C

6.2.5. X-Ray diffractometry

Due to the promising CV data, XRD measurements are performed to determine the exact composition of the active material. The diffraction measurements confirm the presence of two sodium titanate phases as well as a small fraction of rutile or anatase.

Table 5 Phase composition of the active material

Annealing Temperature [°C]	**850**					
Rinsing Steps	**2**	**3**	**4**	**5**	**6**	**7**
$Na_2Ti_6O_{13}$ [%]	6	42	83	64	47	53
$Na_2Ti_3O_7$ [%]	94	58	0	0	0	0
TiO_2 Rutile [%]	0	0	17	36	53	47

Table 5 clearly shows the disappearance of the 'high capacity' $Na_2Ti_3O_7$ phase after 4 steps of rinsing, as referred to Senguttuvan et al. in *Chemistry of Materials* in 2011, and the rise of a 'low capacity' $Na_2Ti_6O_{13}$ phase with increasing number of rinsing steps. At 4 or more rinsing repetitions no 'high capacity' phase can be detected, as predicted by the CV diagram depicted in Figure 15. Instead of leaving only the 'low capacity' phase, a new rutile phase is formed when performing more rinsing repetitions. Figure 19 depicts a comparison of the whole rinsing step spectrum prepared at an annealing temperature of 850°C. The formation of the rutile phase as well as the decrease of the $Na_2Ti_3O_7$ phase is apparent at first glance. It is clearly indicated by a strong decrease of the peaks at 10.66 and 16 positions and the striking rutile peak at 27.54 gathered from the seven times rinsed sample.

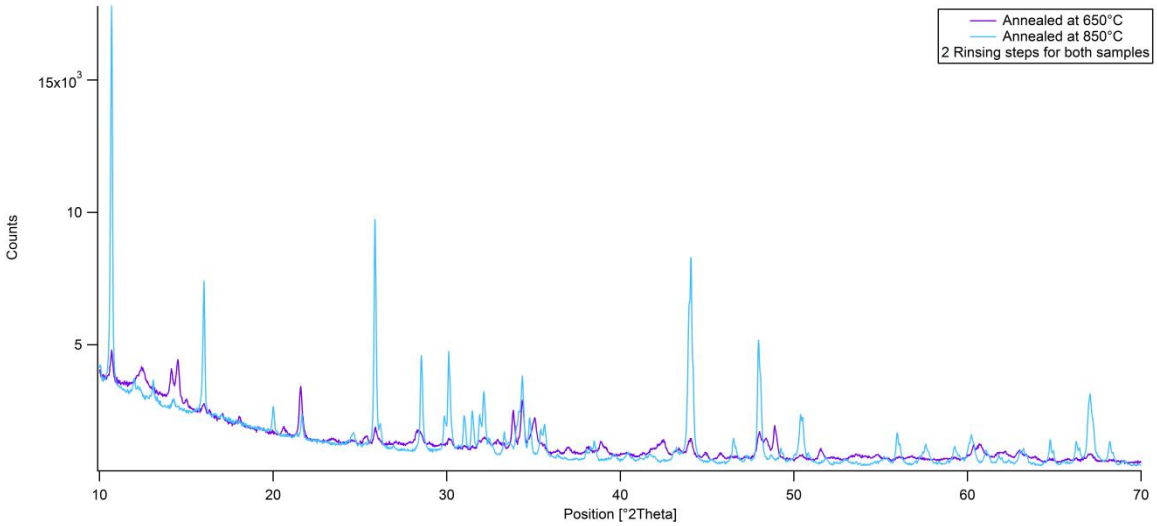

Figure 19 XRD comparison of samples rinsed 2 times with different annealing temperatures

Figure 20 displays a comparison of two times rinsed samples which are annealed at 650 and 850°C respectively. Due to the fact that only a small fraction of the investigated material, numerical 9.7%, could be identified as $Na_2Ti_3O_7$ phase, the peaks gathered from this material are significantly smaller than those obtained from the 850°C annealed sample that shows a $Na_2Ti_3O_7$ content of 94%. Nevertheless similarities of the two spectra can clearly be seen in this diagram. An investigation of the TiO_2 educt reveals a composition of 88% anatase and 12% rutile.

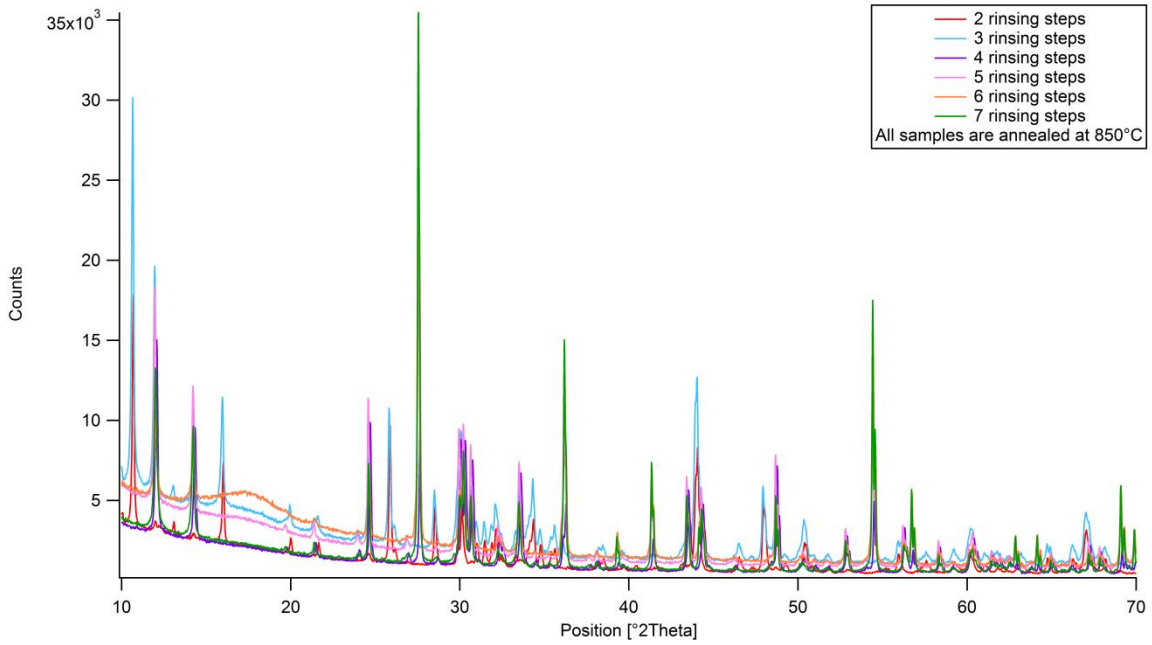

Figure 20 XRD measurement of all rinsing steps at 850°C annealing temperature

6.2.6. Galvanostatic Cycling with Potential Limitation

Galvanostatic cycling is carried out to investigate the long period cycling performance of the prepared active materials in a half-cell assembly with sodium metal cathode and reference electrode. As mentioned in the experimental setup part 1M $NaClO_4$ in PC is used as electrolyte. The cells are cycled with cycling rates of 40mA/g and 200mA/g, switching from 40 to 200mA/g after 50 cycles. The change in cycling rate can easily be recognized in the change of specific capacity as well as in the Coulombic efficiency diagrams by an immediate increase of either capacity or efficiency. Due to the fact of evaluating the rinsing medium, galvanostatic cycling for materials rinsed with each of the three media is performed.

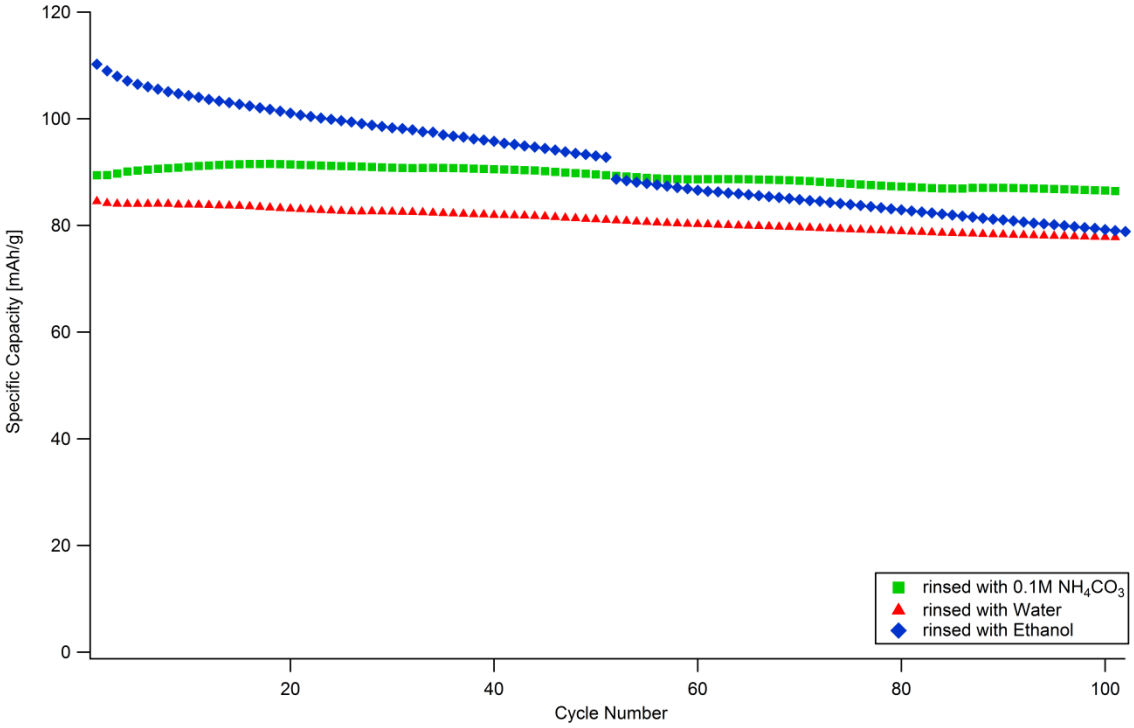

Figure 21 Specific capacities of active materials rinsed with different solvents

The results depicted in Figure 21 and 22 show that either water or 0.1M $(NH_4)_2CO_3$ deliver active materials with suitable performance for long-term utilization in sodium cells. The 0.1M $(NH_4)_2CO_3$ rinsing method is picked for further investigations, because of its advantage of providing an active material with higher stability and specific capacity (seen in Figure 21). As shown in Figure 22, reversibility of water and 0.1M $(NH_4)_2CO_3$ rinsed active materials is roughly the same. Further investigations are performed with samples annealed at 850°C that are differing in rinsing steps. It is obvious that samples

containing the 'high capacity' $Na_2Ti_3O_7$ phase show a significantly higher specific capacity than samples rinsed more than 3 times.

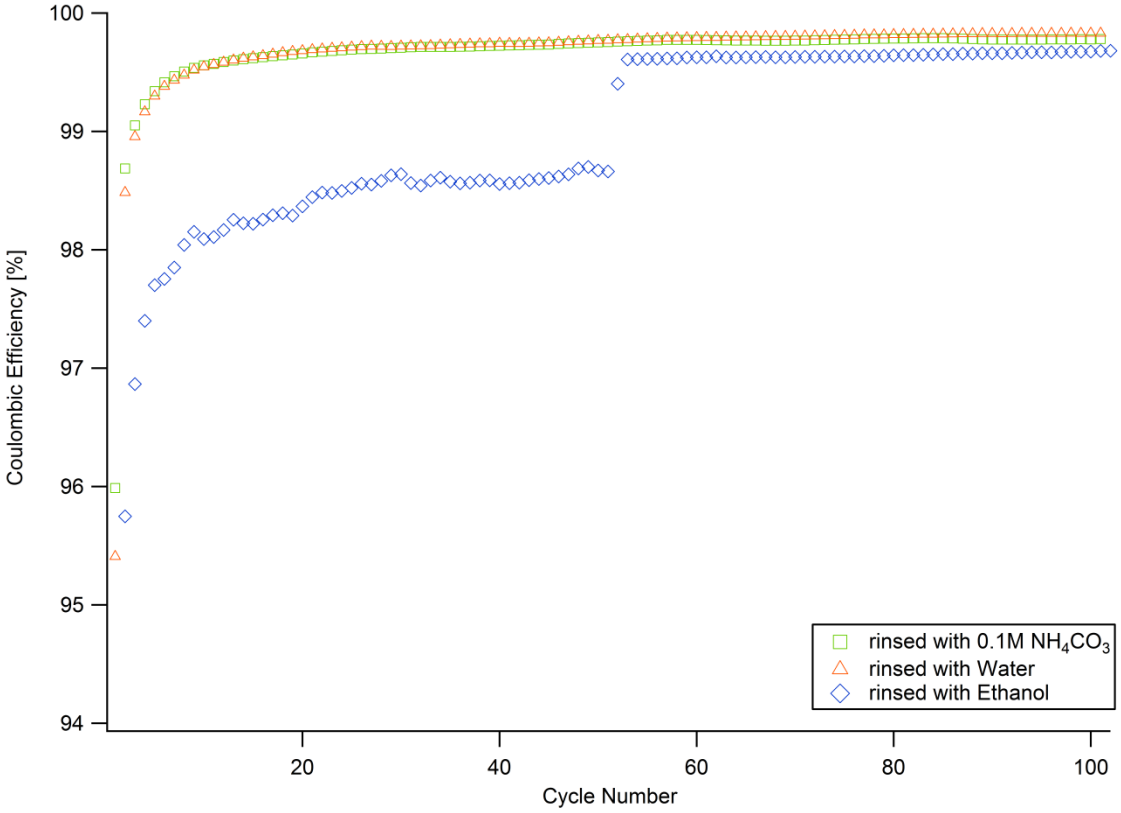

Figure 22 Comparison of efficiency of the materials resulting from different rinsing solvents

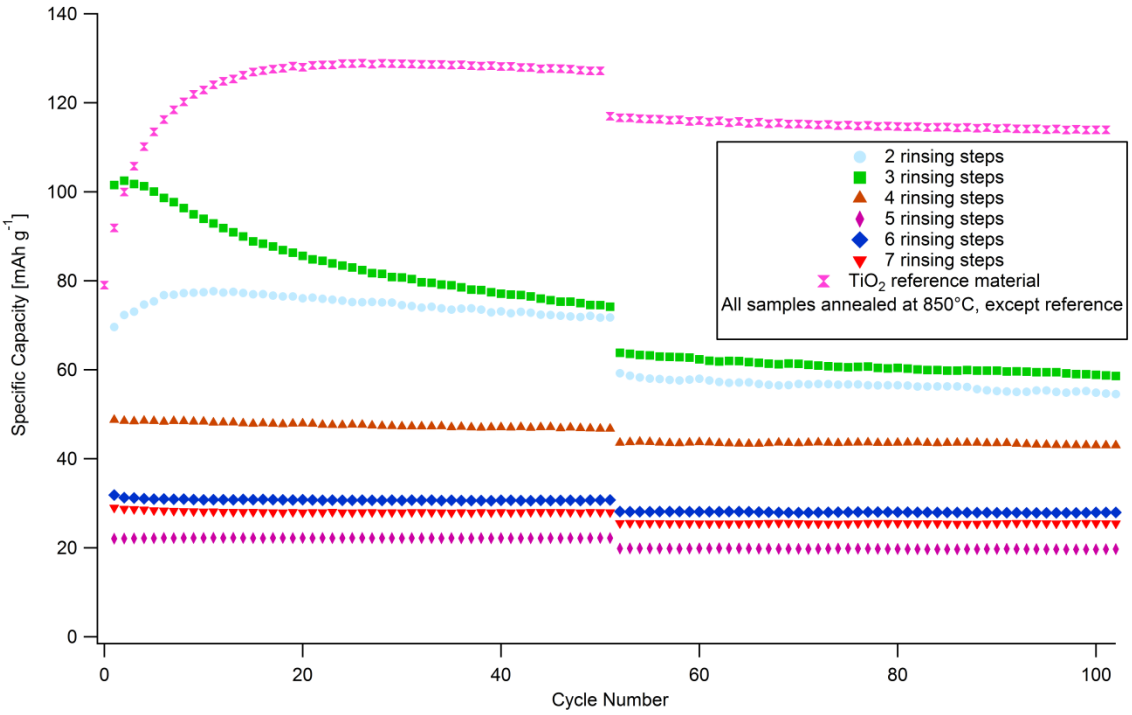

Figure 23 Cycling of materials with different rinsing repetitions and reference material

This effect does not only occur at low cycling rates, but also at cycling rates as high as 200 mA/g. All the aforementioned details as well as the comparison to the TiO_2 rutile/anatase educt can be seen in Figure 23. The educt is prepared in the same way to ensure comparability and reproducibility. Curiously the as-prepared TiO_2 reference shows higher specific capacities than the hydrothermal synthesized materials. This might be due to the higher specific surface caused by particles with sizes lower than 5nm, which enables the material to intercalate more sodium ions. Nevertheless, a comparison of Coulombic efficiencies of both materials, as seen in Figure 24, reveals an enormous lack in reversibility of the as-prepared educt electrode. Therefore it can be assumed that the hydrothermal synthesized material, which is refined by 2 rinsing steps and annealed at 850°C, is the most suitable for anode applications in sodium ion batteries. Figure 24 also shows that the most reversible and therefore most stable material obtained during this work is the almost 1:1 mixture of rutile and 'low capacity' $Na_2Ti_6O_{13}$ phase. Even though the reversibility of the materials obtained after 2 and 3 rinsing repetitions and an annealing process at 850°C is not as high as the 'low capacity' phase mixture, it is still above 99% and seems to stabilize at a value of almost 99.5%.

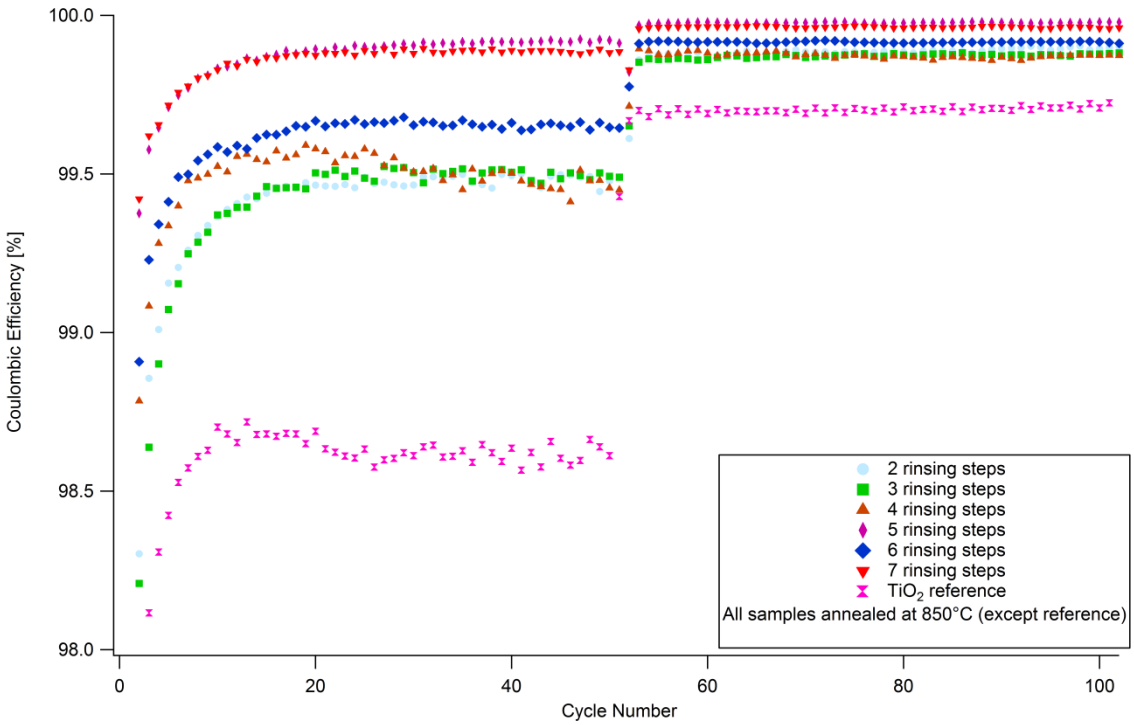

Figure 24 Coulombic Efficiency of materials undergoing different numbers of rinsing repetitions and a reference material

7. Conclusions and outlook

This thesis targets the lack of suitable high capacity anode materials for sodium-ion battery applications. It does not only focus on finding new materials by using alternative synthesis methods, but also aims at a straightforward synthesis process that is easily reproducible. In order to do so, the synthesis products $Na_2Ti_3O_7$, $Na_2Ti_6O_{13}$ and TiO_2 are thoroughly compared by using a wide range of analysis methods. The evaluation of 3 different rinsing solvents named 0.1M $(NH_4)_2CO_3$, water and ethanol leads towards the utilization of 0.1M $(NH_4)_2CO_3$, since samples prepared this way show the highest stable specific capacity. Cyclic voltammetry measurements of materials prepared at different annealing temperatures show that the occurrence of the 'high capacity' phase increases with increasing annealing temperature. While the phase does not form at temperatures of up to 650°C, its share shows an increasing trend from 650°C upwards. SEM investigations show that the structure of the prepared material appears to be a pile of rods that seem to order themselves when raising annealing temperature. The length of the rods is in micrometer scale and their diameter is in the nanometer range. XRD measurements reveal the 'high capacity' phase to be $Na_2Ti_3O_7$ and also show the disappearance of the phase with increasing numbers of rinsing repetitions. The formation of a rutile phase at more than 3 rinsing steps can also be verified by XRD measurements. In order to find a production method of a high purity phase of $Na_2Ti_3O_7$, the hydrothermal synthesis coupled with 2 rinsing steps using 0.1M $(NH_4)_2CO_3$ as solvent and an annealing process at 850°C yields a material with 94% 'high capacity' fraction. Further investigations performed by galvanostatic cycling with potential limitation state that a specific capacity of 72 mAh/g and 58 mAh/g, at 40 and 200 mA/g respectively, can be achieved for the as-prepared material. The Coulombic efficiency of the same material reaches 99.47% after 20 cycles at 40 mA/g and 99.89% after 55 cycles at 200 mA/g. The increased efficiency can be explained by the faster in and exertion of the sodium ions in the structured electrode material. The sodium ions do not have as much time to spread into the material as during the 40 mA/g experiment phase. Further investigation of the material, especially focused on the intercalation of the sodium ions in the structure, needs to be performed to adapt the production process to achieve higher specific capacities.

8. Bibliography

[1] Michael D. Slater, Donghan Kim, Eungje Lee, Christopher S. Johnson; Sodium-Ion Batteries; Adv. Funct. Mater. 2013, 23, 947-952

[2] Michael D. Slater, Donghan Kim, Eungje Lee, Christopher S. Johnson; Sodium-Ion Batteries; Adv. Funct. Mater. 2013, 23, 947

[3] V. L. Chevrier, G. Ceder; Challenges for Na-ion Negative Electrodes; J. Electrochem. Soc. 2011 , 158

[4] Oh, S. M.; Myung, S. T.; Jang, M. W.; Scrosati, B.; Hassoun, J.; Sun, Y. K.; An advanced sodium-ion rechargeable battery based on a tin-carbon anode and a layered oxide framework cathode. PCCP 2013, 15, 3827-3833

[5] Alcantara, R.; Jimenez-Mateos, J. M.; Lavela, P.; Tirado, J. L., Carbon black: a promising electrode material for sodium ion batteries. Electrochem. Commun. 2001, 3, 639-642

[6] Ponrouch, A.; Goni, A. R.; Palacin, M. R., High capacity hard carbon anodes for sodium ion batteries in additive free electrolyte. Electrochem. Commun. 2013, 27, 85-88

[7] Naylor, B. F., High-Temperature Heat Contents of Na2TiO3, Na2Ti2O5 and Na2Ti3O7. J. Am. Chem. Soc. 1945, 67, 2120

[8] Senguttuvan, P.; Rousse, G.; Seznec, V.; Tarascon, J. M.; Palacin, M. R., Na2Ti3O7: Lowest Voltage Ever Reported Oxide Insertion Electrode for Sodium Ion Batteries. Chem. Mater. 2011, 23, 4109-4111

[9] Zárate, R.A.; Fuentes, S.; Wiff, J.P.; Fuenzalida, V.M.; Cabrera, A.L., Chemical composition and phase identification of sodium titanate nanostructures grown from titania by hydrothermal processing. Journal of Physics and Chemistry of Solids 2007, 68, 628–637

[10] Lin, Y. M.; Abel, P. R.; Gupta, A.; Goodenough, J. B.; Heller, A.; Mullins, C. B., Sn-Cu Nanocomposite Anodes for Rechargeable Sodium-Ion Batteries. ACS Appl. Mater. Interfaces 2013, 5, 8273-8277

[11] Xiao, L; Cao, Y.; Xiao, J.; Wang, W.; Kovarik, L.; Nie, Z.; Liu, J., High capacity, reversible alloying reactions in SnSb/C nanocomposites for Na-ion battery applications. Chem. Commun. 2012, 48, 3321-3323

[12] Recham, N.; Chotard, J. N.; Dupont, L.; Djellab, K.; Armand, M.; Tarascon, J. M., Ionothermal Synthesis of Sodium-Based Fluorophosphate Cathode Materials. J. Electrochem. Soc. 2009, 156, A995

[13] Chihara, K.; Kitajou, A.; Gocheva, I. D.; Okada, S.; Yamaki, J., Cathode properties of $Na_3M_2(PO_4)_2F_3$ (M=Ti, Fe, V) for sodium-ion batteries. J. Power Sources 2013, 227, 80-85

[14] McCarley, R.E.; Lii, K.H.; Edwards, P.A.; Brough, L.F., J. Solid State Chem. 1985, 57, 17

[15] Tarascon, J. M.; Hull, G. W., Sodium Intercalation into the Layer Oxides $Na_xMo_2O_4$. Solid State Ionics 1986, 22, 85-96

[16] Kim, D.; Lee, E.; Slater, M.; Lu, W.; Rood, S.; Johnson, C.S., Layered $Na[N_{i0,33}Fe_{0,33}Mn_{0,33}]O_2$ cathodes for Na-ion battery application. Electrochemistry Communications 2012, 18, 66-69

[17] Ponrouch, A.; Dedryvere, R.; Monti, D.; Demet, A. E.; Mba, J. M. A.; Croguennec, L.; Towards high energy density sodium ion batteries through electrolyte optimization. Energy. Environ. Sci. 2013, 6, 2361-2369

[18] Baur, J.E. in Handbook of Electrochemistry; Zoski, Cynthia G.,Ed;Elsevier:Amsterdam, 2007, 843-844

[19] Denuault, G.; Sosna, M.; Williams, K.-J. in Handbook of Electrochemistry; Zoski, Cynthia G.,Ed;Elsevier:Amsterdam, 2007, 438-441

[20] Brown, T.L.; LeMay, H.E.; Bursten, B.E. in Chemistry: The Central Science; Pearson Education, Inc.:München, 2006, 545

9. Appendix

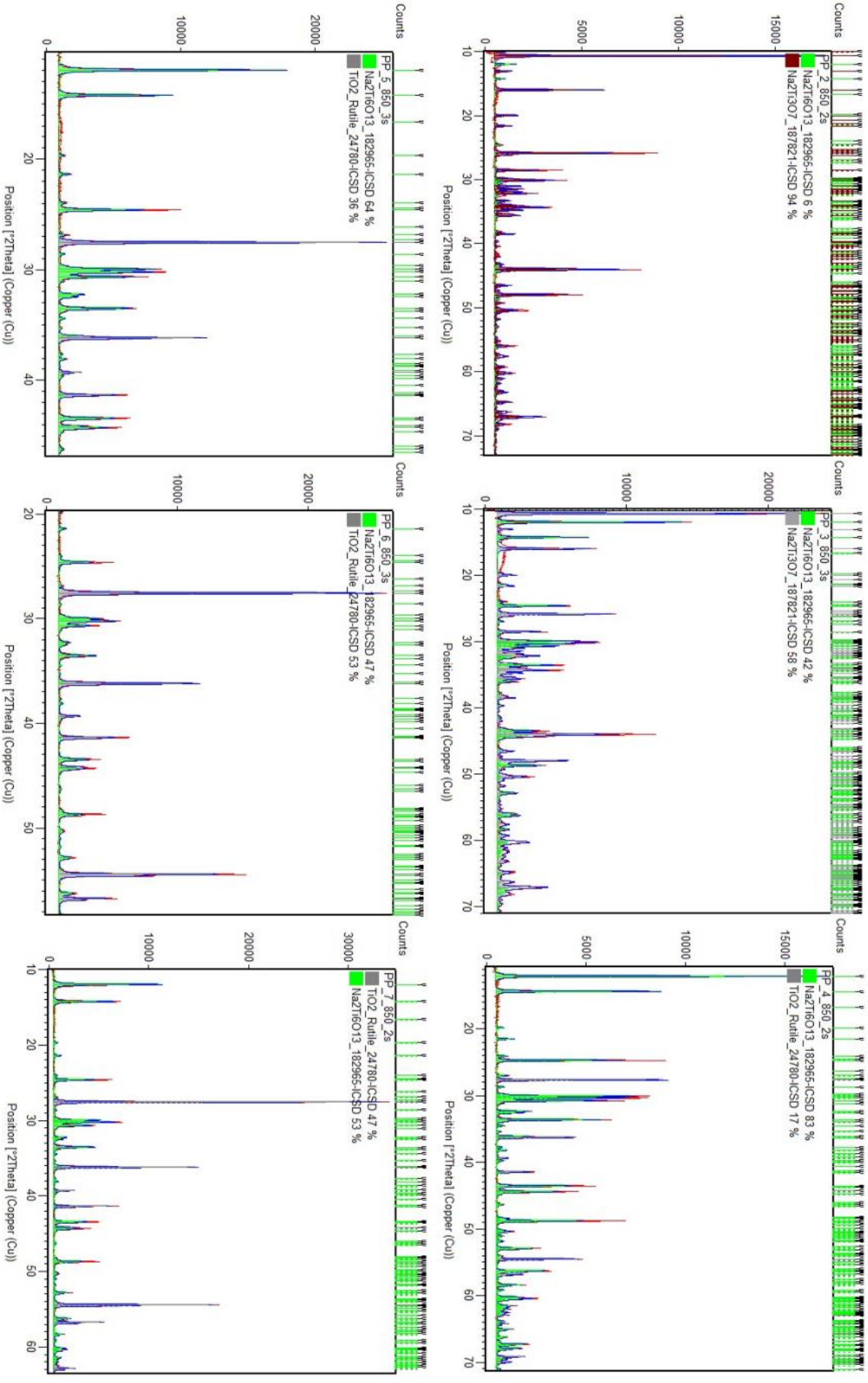

Figure 25 Comparison of XRD data gathered for samples annealed at 850°C and undergoing different rinsing repetitions

AFFIDAVIT

I declare that I have authored this thesis independently, that I have not used other than the declared sources/resources, and that I have explicitly indicated all material which has been quoted either literally or by content from the sources used. The text document uploaded to TUGRAZonline is identical to the present master's thesis.

Date	Signature